# Applicability of multispectral Sentinel data for mineral exploration by use of remote sensing and geospatial technologies

## A case study in Northern Chile

**Edmundo Tulcanaza**

**jtulcana@uni-muenster.de**

A thesis submitted in fulfilment of the requirements for the award of the Degree of Master of Science (Geospatial Technologies)

| | |
|---|---|
| **Dissertation supervised by:** | **Dr. Torsten Prinz** |
| **Co-supervisors:** | **Dr. Hanna Meyer** |
| | **Dr. Joaquín Torres** |

**Institut für Geoinformatik der Universität Münster**

**February 2022**

# DECLARATION

I declare that this thesis entitled, "Applicability of multispectral Sentinel data for mineral exploration by use of remote sensing and geospatial technologies. A case study in Northern Chile", is a summary of my own investigation, exception made of public information which has been cited in the references. The thesis has not been accepted for any degree and is not concurrently submitted in candidature of any other degree.

**Signature:** 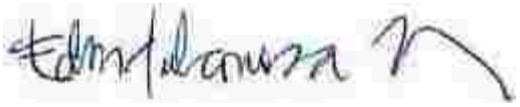

**Name:** Edmundo Tulcanaza

**Place:** Münster, Germany

Date: 24th February 2022

# ACKNOWLEDGMENT

Firstly, I want to deeply thank my supervisor, Dr. Torsten Prinz, for his valuable supervision and guidance. I would like to thank him for helping me in focusing the topic selected for this thesis, for provide me software information for remote sensing applications, and for always assisting me in keeping my energy and encouragement in pursuit of my goal. I would like also to thank my Co-supervisors, Dr. Hanna Meyer and Dr. Joaquín Torres. Dr. Meyer for call my attention when it was need it, and Dr. Torres for his always willingness to help me in the face of any technical obstacle in the context of my thesis.

I would also like to offer my deepest gratitude to every professor of the Emeritus Mundus program to whom I had the privilege to know through the series of course-work I attended in the context of the Geospatial Technologies program. I would like to represent this acknowledgment in Dr. Marco Painho for his support, assistance, and permanent guidance no matter where we are. Furthermore, I would like to thank the authority of Institute for Geoinformatics (IFGI) and Westfälische Wilhelms-Universität Münster (WWU) for providing me with the resources and facilities to complete this work. Finally, I want to express my heartfelt appreciation and thanks to my families, colleagues, and friends for supporting me in completing this project. My virtual presence among them has been solely motivated in the pursuit of my goal.

# ABSTRACT

The objective of this MSc thesis is to prove that the Sentinel-2 satellite has the same capabilities for mineral exploration than another satellite considered the “reference technology” by the minerals industry. Since there have been an extensive use and applications of the Landsat-8 satellite for mineral exploration, this satellite is considered in this case the “reference technology”.

To prove the capability of the Sentinel-2, a sequence of key applications applied on the Landsat-8 satellite for mineral exploration have been carried out using the Sentinel-2 on a specific mine site. Mine site for this investigation is the Escondida mine in northern Chile. Through several remote sensing applications such as band combinations, band ratios, PCA analyses, and pixel´s classification both satellites, Landsat-8 and Sentinel-2 have been tested on Escondida and results have been obtained and discussed.

As a conclusion of this analysis, the capability of Sentinel-2 for mineral exploration has been proved, potential improvements have been identified and limitations in its prospective use have been indicated**.**

# TABLE OF CONTENTS

# List of Figures

# Tables

# Applicability of multispectral Sentinel data for mineral exploration by use of remote sensing and geospatial technologies A case study in Northern Chile

**Edmundo Tulcanaza**

## 1 Introduction

As the title of this document implies, the central objective of this thesis is to evaluate the applicability of the sensor Sentinel-2 for mineral exploration. To confirm that Sentinel-2 satellite is completely applicable for mineral exploration, it is necessary to confront it against another one which completely delivers a proven remote sensing technology in mineral exploration. Having selected this "reference technology", Sentinel-2 should replicate the current methodology offered by this "reference technology" at a similar or better level of competence. At present, Landsat-8 is the satellite that has been used extensively in mineral exploration across the world in many arid and non-arid regions, with efficiency, and remarkable success. Due to the successful history of Landsat-8´s applications in mineral exploration, including some applications in Chile (***N. Ott et al, 2006; J-C Kim et al, 2014; N. Biswajit et al, 2019***), Landsat 8 will be considered the "reference technology".

Remote sensing today and its association with land imaginary techniques allow the visualization of large land spaces where special features of the earth crust can be visualized

and parameterized. In the face of the opportunities offered by the Chilean ground, the efforts in using remote sensing for mineral exploration have not been too explicit to profit from the multiple features, patterns, and footprints of the Chilean mineralized soil. Contrary to other parts of the world, on which remote sensing applications have been applied to the search of hidden objects such as art works (***F. Monna et al, 2014***), mineral deposits (***N. Ott et al, 2006***), and others, there have been only a few applications of remote sensing along the mineralized Chilean belts (***C. Borie et al, 2019; F. Sabins, 1999;***). A research paper has been written on remote sensing on the Escondida mine (***N. Ott et al, 2006***) which is the largest copper-molybdenum mine in the world.

Mineral exploration is a capital intensive and complex activity. Finding an orebody take distinctive types of material resources, time, and monies. This is the reason why remote sensing is becoming a tool to provide crucial information at a very low cost.

Today, mineral exploration is a very dynamic area in the mineral industries. It is very dynamic because the present world´s intention of changing the energy sources (from fossil oriented to electro-mobility oriented) will depend largely on finding more minerals and metals (copper, lithium, nickel, cobalt, and others for manufacturing large batteries stocks). The pace at which these minerals and metals are found, at present, is not sufficient to match their requirements in the future.

In Chile, the largest world´s copper producer, as well as in other mining countries, mineral exploration has been at one of its lowest levels in years and remote sensing has not been very much used. This has been one of the motivations in choosing this topic. For implementing this investigation, a review of papers and technical documentation on the basic definitions of remote sensing have been revised and summarized in the Appendix citing their authors identification and/or original publications link.

Following, I will briefly characterize the geological nature of the Escondida district, looking into the geological nature of this deposit which has been subjected to a hydrothermally altered

process generating an assemblage of different mineralized family units in accord with the various phases of the deposit´s source.

A work flow of this thesis will be implemented below to conduct similar tasks for both satellites. Work flow will include implementation of band composition, band ratios, PCA analysis, spectral indices, and pixels classification along with results, comments, and discussions.

Through this juxtaposition of Landsat-8 and Sentinel-2 performances, it is my opinion that the latter is completely capable to perform the same type of activities for mineral exploration than the former.

## 2. Methods and Materials

### 2.1 Study area

Escondida mine, as a porphyry copper-molybdenum deposit subjected to hydrothermal alteration, has developed in different alteration phases among them

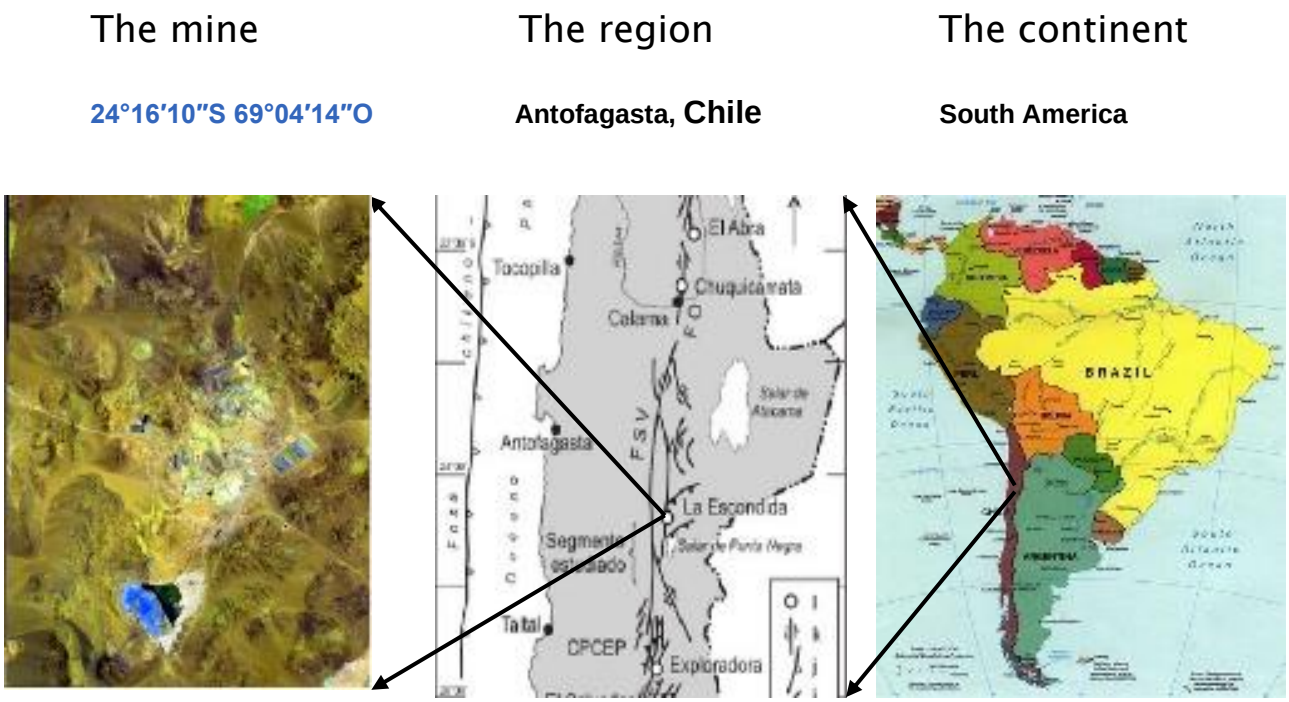


***Figure 1: Escondida Location in Northern Chile, Antofagasta region, South America,***

The Escondida mine is located in a arid area in Northern Chile, Figure 1. It belongs to the copper belt that runs along the country where most of the huge Chilean copper deposits are located along one of the most important geological fault of the country: the West Fault (Domeyko Cordillera).

The Escondida´s mineralization and alteration was developed in three separated stages of geological activity: the first was a pervasive and fracture controlled alteration including an inner potassic and an outer propylitic zones. The second phase is a chlorite-sericite-quartz alteration zone. Finally, the third phase is constituted by a rhyolite intrusion and an advanced argillic alteration distributed in accord with the main fault zones, and by the contacts between the rhyolites and other intruded rocks. Alteration is defined by pyrophyllite, alunite and quartz, and abundant high sulphidation assemblages (***PorterGeo Database, 2021***).

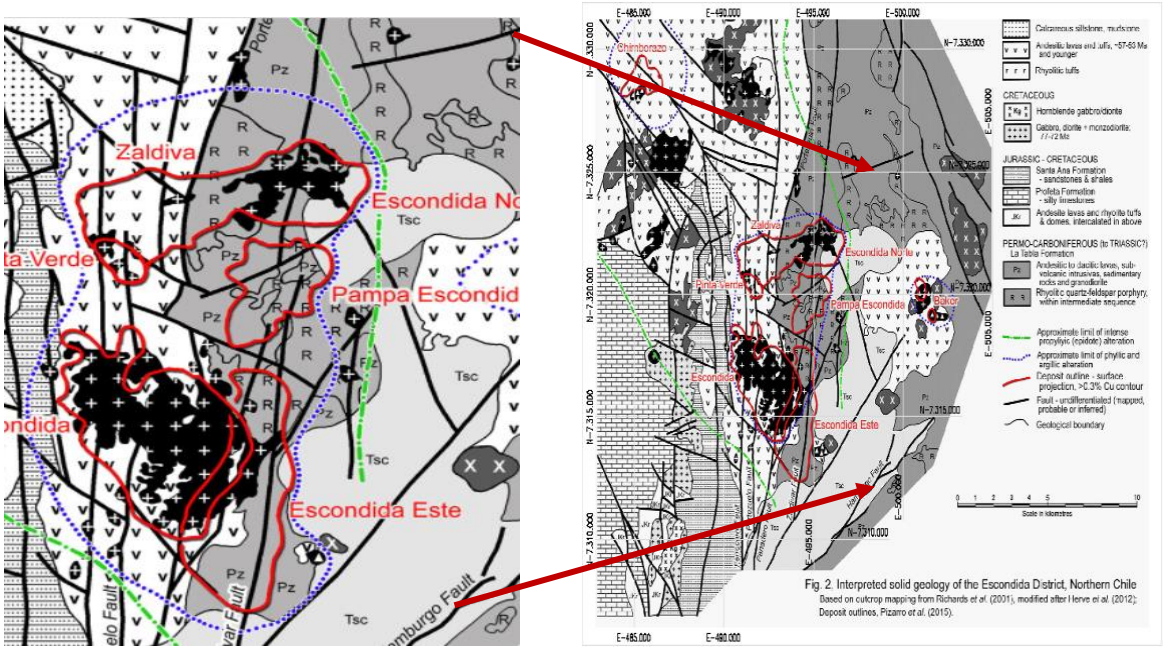


***Figure 2. Escondida Geological map as an interpreted solid geology of the Escondida Districtct, Northern Chile, based on outcrop mapping from J.P. Richards and others (2001), modified by M. Hervé and others (2012). Deposit outlines by A. Pizarro and others (2015) in accord with Porter GeoEscondida. 2021.***

Important for this investigation is the blue-dashed line in the left map indicating the aura where the argillic alteration (final alteration phase) is concentrated on the present surface

## 2.2 Data acquisition

To conduct the task of assessing the applicability of the Sentinel-2 spacecraft in mineral exploration activities, the "reference technology" to look upon will be the normal sequential activities followed by Landsat-8 for the normal activities in mineral exploration.
First activities and materials preparation.
Among the first activities to develop were:

▪ Opening accounts for the acquisition of land cover (Escondida district) images at:

- **USGS Global Visualization Viewer, and at the**
- **Europe's Copernicus programme.**

Images of the Escondida district were obtained for Landsat- 8 (2016-03-3) and Sentinel-2 (2016-03-5). During March there are few clouds in the district´s sky. Actually, images with less than 10% of clouds were chosen.

▪ Selecting geology and mineralogy maps of La Escondida district.

▪ Setting the "reference technology". This technology will be set up by using data reported in the paper "GIS Analyses and Favorability Mapping of Optimized Satellite Data in Northern Chile to improve exploration for mineral copper deposits". (***Norbert Ott et al, 2006***).

▪ Preparing the systems to be used for the analysis of both Landsat-8 and Sentinel-2 through Pre-Processing that assures to have reflectance values at a Top of Atmosphere (TOA) level for both satellites including geometric, atmospheric, and radiometric corrections. In the case of Lamdsat-8, selection was Level 1C similar to the characteristics of Sentinel- 2 selection Level 2A.

▪ GIS Software: ArcGIS Pro version 2.8.0 and QGIS 3.16.3 were used.

## 2.3 Methodology workflow

In accord with various references indicated in the Bibliography, most of the applications in mineral exploration using remote sensing are based on the following techniques:

**band composition, band ratios, PCA, spectral indices and classification.**

After the application of each of the techniques, results and a discussion will be done.

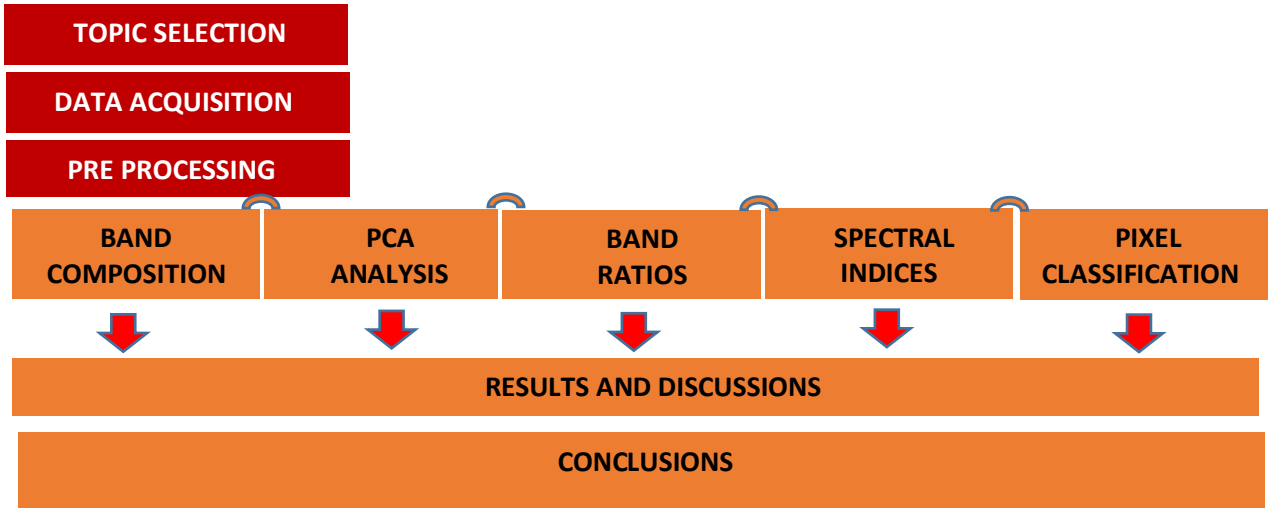


***Figure 3. Workflow started with Topic Selection, Data Acquisition, and Pre Processing procedures and following with five remote sensing techniques. In each case results are discussed for final conclusions at the end.***

The bases for the application of these techniques are presented in the Appendix.

- **band compositions** were used for a first visualization of the whole Escondida district, the purpose being to see the capability of geological discrimination of both satellites. Three different imaginary scenes were used
- **PCA analysis** was used to distinguish more in detail the geological structure of the mineralization assemblage in one of the well-established hydrothermal altered zone. This technique is not only used to maximize variabilities in some few independent components and to reduce data dimensionality but it is also used to contrast the characterization between neighbor bands to better mark discrimination between their mineralization units.

- **band ratios** are math formulae, expressed as a division operation where the numerator is normally of band with the smaller reflectance value and the denominator is the band with the higher reflectance value. The use of a band ratio is to enhance the difference between band-color to mark their separation.
- **spectral indices** are specific combinations of spectral reflectance of two or more wavelengths with the purpose of identifying an object of interest.
- Classification is the process for grouping of pixel indicating similar nature.

Based on these techniques, the juxtaposition of Landsat-8 and Sentinel-2 will be examined.

## 3. Results and Discussion

### 3.1 Band Composition

The first visualization of Escondida will be assuming a natural or true color composite which is an image displaying a combination of visible red, green and blue bands to the corresponding red, green and blue channels on the computer. In both cases the RGB set is red-green-blue (4-3-2).

A composite band is the combination of three image bands into one picture by displaying each band as either red, green or blue color. On the other hand, a false color image is a representation of a multi-spectral image produced using bands other than visible red, green and blue as the red, green and blue components of an image display. False color composites allow us to visualize wavelengths that the human eye cannot see (i.e. near-infrared). In Escondida, I used three compositions RGB because of their reference in literature *(**A. El Atillah, 2019**)*.

Visualizations of images provided by both satellites, at a large scale, are very coincident. Colors differ somehow presumably because of the different wavelengths ranges between both satellites or because of the time difference between the two images. However, in both, the present pits are well shown and roads and terrain topography are similarly sufficiently viewed. Following, the three band combinations will be shown below.

a. SWIR 2 RED BLUE (7 4 2) for Landsat 8 ; (12 4 2) for Sentinel-2

b. SWIR 1 SWIR 2 RED (6 7 4) for Landsat 8 ; (11 12 4) for Sentinel 2

c. SWIR 2 SWIR 1 BLUE (7 6 2) for Landsat 8; (12 11 2) for Sentinel 2

Landsat 8 /2016 03 03 Sentinel 2 /2016 03 05

| bands | wavelength range (μm) | bands | wavelength range (μm) |
|---|---|---|---|
| B 4 | 0.636 – 0.673 | B 4 | 0.646 – 0.685 |
| B 3 | 0.533 – 0.590 | B 3 | 0.537 – 0.582 |
| B 2 | 0.452 - 0.512 | B 2 | 0.439 – 0.535 |

***Figure 4. Band composition of natural color of the Escondida district. Landsat-8 image (03-3-2016) and Sentinel-2 (05-3-2016). Wavelength ranges (μm) are indicated.***

The set of bands 7-4-2 (RGB) in the Landsat-8 image and the set 12-4-2 in the Sentinel-2 image discriminate the study area in two large portions. The portion to the left (red color), in both images, characterized by B7 and B12 respectively appear to show mostly the presence of clay minerals such as sericite, chlorite, biotite, k-felspar, montmorillonite, and others which absorb radiation much more than they reflect it. Band B4 in both images, to the right, relate more to vegetation which is not of interest in this case. However, its reflectance is similar to

that of iron oxide minerals (***D. F. Ducart, 2016***). B2, blue, in both images (right portion), appears to show more iron oxides specimens (magnetite, hematite, pyrite) which absorbs energy.

a

**Landsat 8 /2016 03 03**
**B7 4 2**

**Sentinel 2 /2016 03 05**
**B12 4 2**

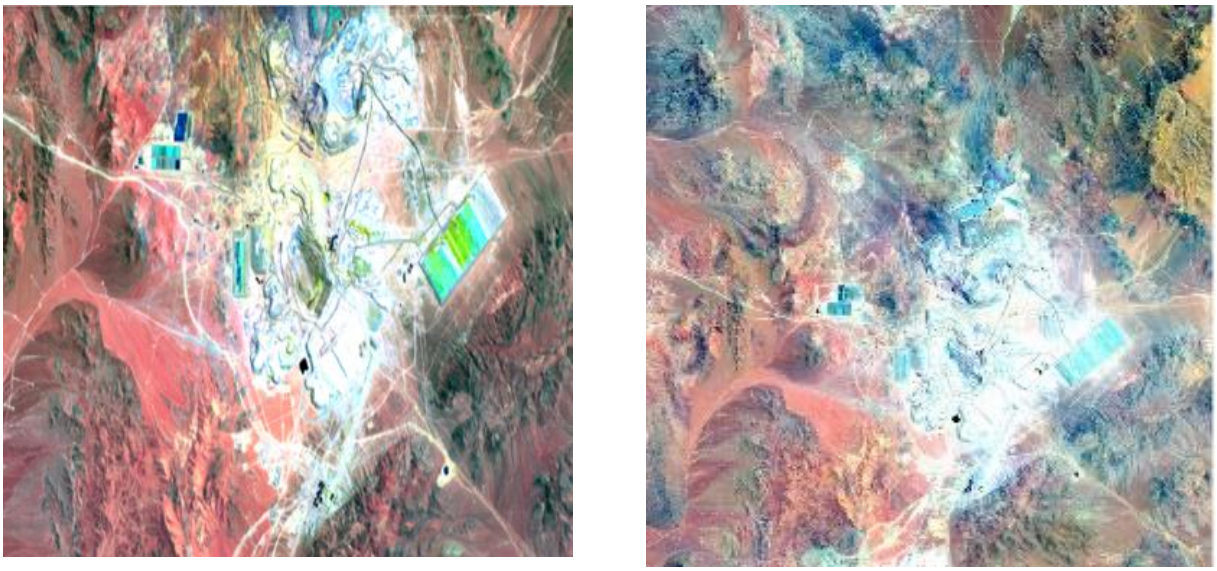

| bands | wavelength range (μm) | bands | wavelength range (μm) |
|---|---|---|---|
| B 7 | 2.201 – 2.294 | B 12 | 2.072 – 2.312 |
| B 4 | 0.636 - 0.673 | B 4 | 0.646 - 0.685 |
| B 2 | 0.452 - 0.512 | B 2 | 0.439 – 0.535 |

***Figure 5. Band composition SWIR2, Red, Blue of the Escondida district. Landsat-8 image (03-3-2016) and Sentinel-2 (05-3-2016) for geological interpretation. Wavelength ranges (μm) are indicated.***

In the case of Figure 5, delineation of geological structures given by Landsat-8 and Sentinel-2 is not the same affecting the scale of visualization but the pattern of these structures along

with their colors appear very similar in such a way that the geological characterization is unmistakably the same.

.

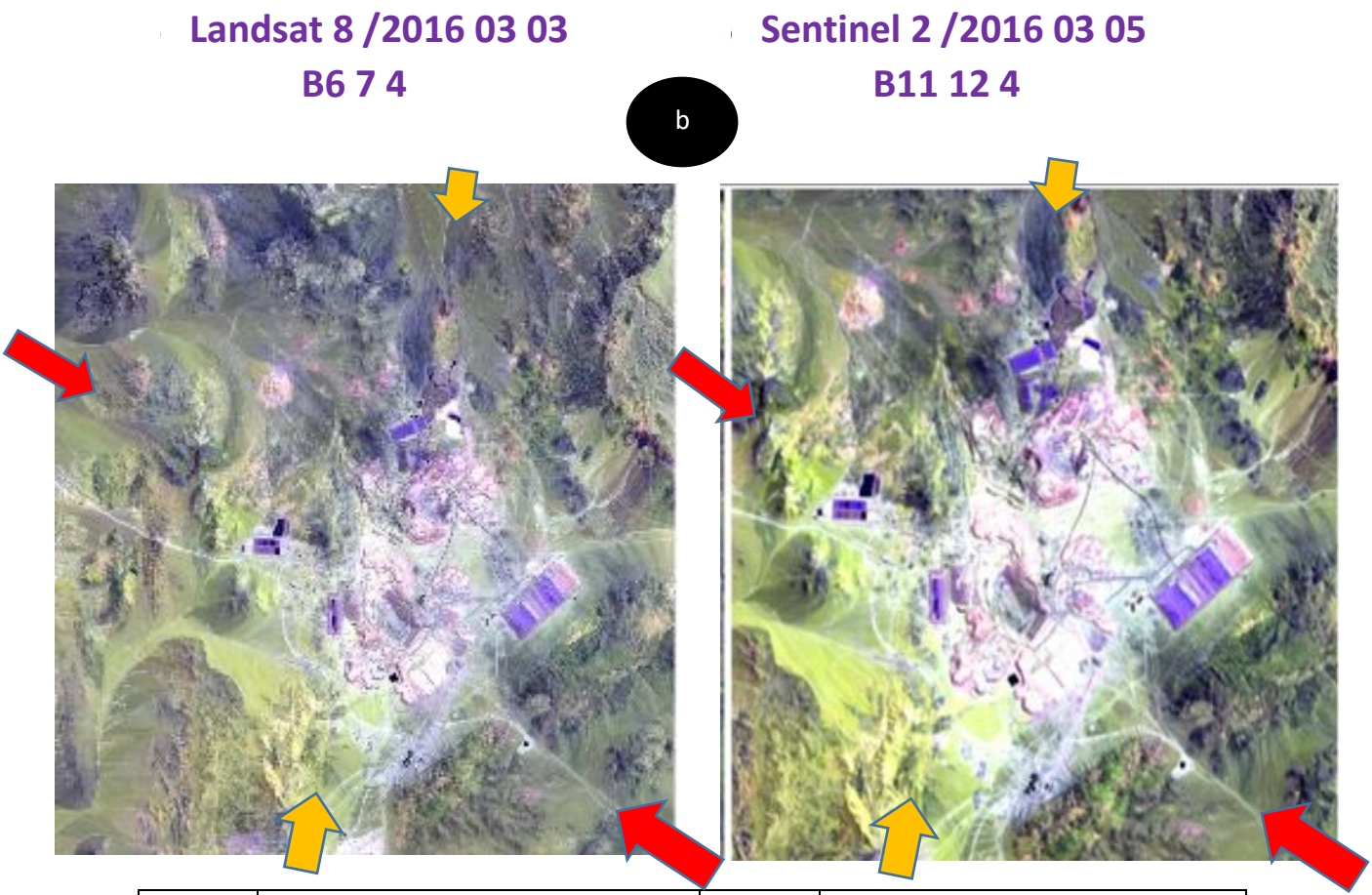


| bands | wavelength range (μm) | bands | wavelength range (μm) |
|---|---|---|---|
| B 6 | 1.567 – 1.651 | B 11 | 1.539 – 1.681 |
| B 7 | 2.201 – 2.294 | B 12 | 2.072 – 2.312 |
| B 4 | 0.636 - 0.673 | B 4 | 0.646 - 0.685 |

***Figure 6. Band composition SWIR2, Red, Blue of the Escondida district. Landsat-8 image (03-3-2016) and Sentinel-2 (05-3-2016) for structural geology interpretation. Wavelength ranges (μm) are indicated.***

In the Escondida district there are at least five major faults one of them being the West Fault that runs all along Northern Chile where the major copper deposits are located (ie, Chuquicamata, Radomiro Tomic, and others). At Escondida, the West fault runs tangential to the mineralized occurrences.

In the Landsat-8 image, Figure 6, spectral bands 6 and 7 as well as in Sentinel-2 image, spectral bands 11 and 12, utilize parts of the Short Wave Infra-Red (SWIR) bands which, in this case, are very useful to identify rocks and soil structures. Band set 6-7-4 (RGB) in Landsat-8 as well as band set 11-12-4 in Sentinel-2 serve to recognize some of the key structural faults in the study area. Finally, a pair of additional bands set were applied

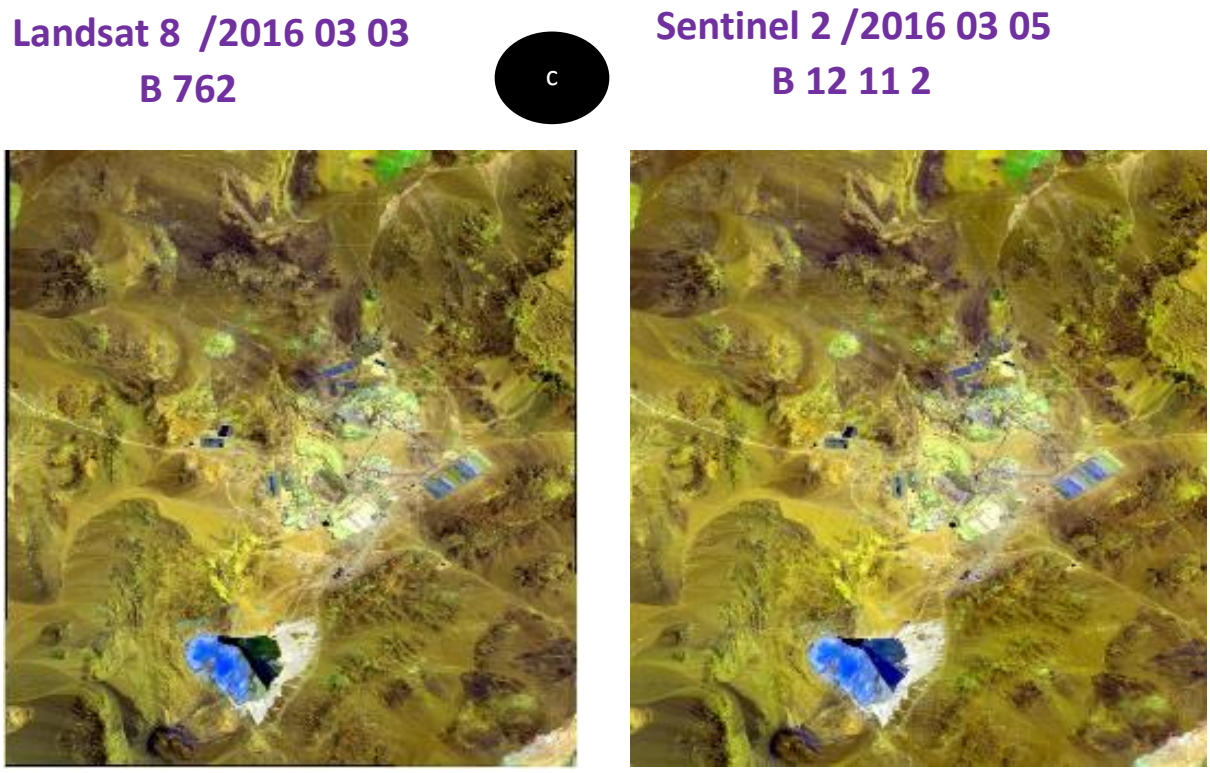


| Bands | wavelength range (μm) | bands | wavelength range (μm) |
|---|---|---|---|
| B 7 | 2.201 – 2.294 | B 12 | 2.072 – 2.312 |
| B 6 | 1.567 – 1.651 | B 11 | 1.539 – 1.681 |
| B 2 | 0.452 - 0.512 | B 2 | 0.439 – 0.535 |

***Figure 7. Band composition SWIR2, SWIR1, Blue of the Escondida district. Landsat-8 image (03-3-2016) and Sentinel-2 (05-3-2016) for macro-geological unit definition and interpretation. Wavelength ranges (μm) are indicated.***

Figure 7 shows, in both cases, a darker stripe towards the north of the Escondida mine. To the south of the image, mineralization exhibits a much higher reflectance than the north portion indicating a significant presence of clay minerals such as, presumably, , alunite, illite and others.

As Figures 4, 5, 6, and 7 showed, the images of both Landsat-8 and Sentinel-2 are very similar.to each other. Some of the features represented on the image gotten with one of these space-craft are somehow replicated in the image of the other. So, in addition to show that both are complementary to each other, a remote sensing technique such as the band composition show the capability of Sentinel-2 to perform at least at the same level than the Landsat-8

## 3.2 Principal Component Analysis (PCA)

The PCA analysis, as viewed in the Appendix, is a statistical method that allows the reduction of available data in a system, in our case a remote sensing data, without loss of the intrinsic characteristics of the original data. Data reduction is achieved through the quantification of the covariance matrix, first, the correlation matrix later, and, finally, through the eigenvectors- eigenvalues matrix.

In this present case, PCA will be used to approach (1) visualization of the mine site and (2) corroboration of mineral specimen identification.

GIS software, normally, provides the eigenvector-eigenvalues matrix with the explained variance. This explained variance encloses the maximum variability portion of the system reached by every component.

Table 1 shows the eigenvalues matrix using the first seven bands of the Landsat-8 satellite along with their explained variance. Figures 8, 9, y 10 show the images of each of the first three components. These contain the maximum variabilities of the system.

| | PC1 | PC2 | PC3 | PC4 | PC5 | PC6 | PC7 |
|---|---|---|---|---|---|---|---|
| **B1** | **-0.2613** | **0.3017** | **0.4627** | **-0.1834** | **0.5153** | **-0.3189** | **-0.4749** |
| **B2** | **-0.2917** | **0.3598** | **0.3840** | **0.1211** | **0.0891** | **0.2366** | **0.7478** |
| **B3** | **-0.3561** | **0.3642** | **0.1069** | **0.0603** | **-0.5913** | **0.4388** | **-0.4278** |
| **B4** | **-0.4095** | **0.2665** | **-0.3577** | **0.0819** | **-0.2979** | **-0.7132** | **0.1701** |
| **B5** | **-0.4147** | **0.0860** | **-0.6559** | **-0.0490** | **0.4947** | **0.3746** | **-0.0518** |
| **B6** | **-0.4811** | **-0.5042** | **0.2536** | **0.6652** | **0.0833** | **0.0069** | **0.0202** |
| **B7** | **-0.3852** | **-0.5603** | **0.0662** | **-0.7045** | **-0.1905** | **-0.0225** | **0.0010** |

Table 1. Principal Components Matrix with Eigenvalue Loadings Landsat-8 on the Escondida district

| Eigenvalues | Explained variance | Cumulative variance |
|---|---|---|
| **0.019948** | **87.360727** | **87.360727** |
| **0.002434** | **10.661100** | **98.021835** |
| **0.000206** | **0.905322** | **98.927157** |
| **0.000145** | **0.637734** | **99.564891** |
| **8.356152 E-05** | **0.365942** | **99.830934** |
| **1.314794 E-05** | **0.057579** | **99.988413** |
| **7.645636** | **0.011586** | **100.** |

Table 2 Eigenvalues and explained variance PCA Landsat-8 – Escondida district

Table 2 shows that the first component, PC1, encloses 87.37% of the total variability; the second PC2 supplied 10.66%: the PC3 reported 0.90% of the total variability. The other PC are insignificant. The first three PCs sum up 98.93**%.**

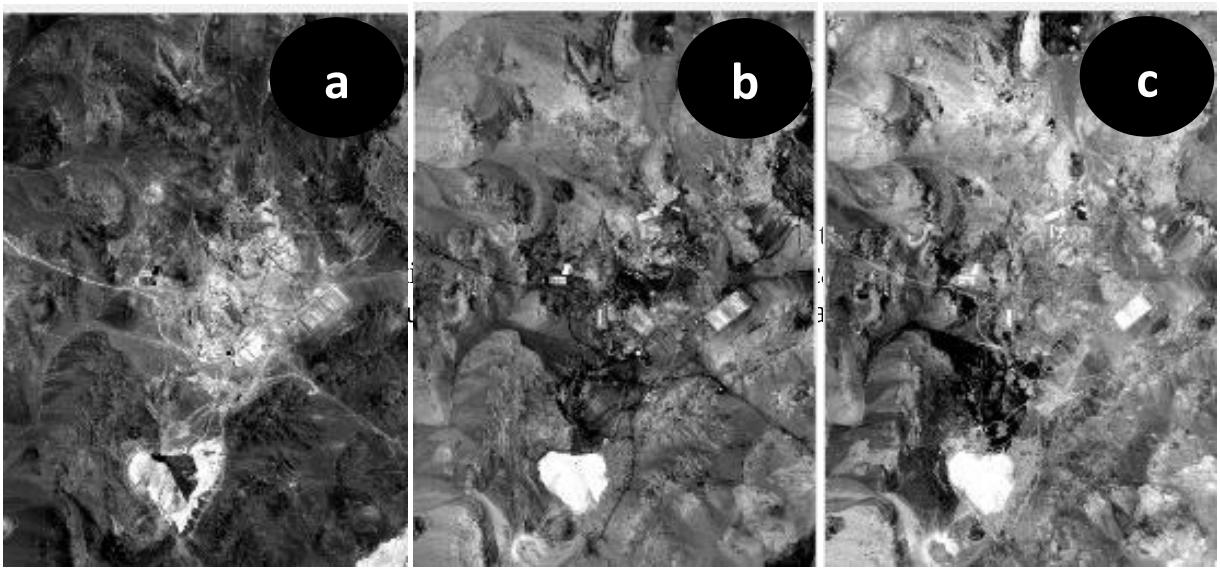


***Figure 8. Visualizations of the first three Components in the PCA analysis on the Escondida district using Landsat 8. (a) first component; (b) second component; (c) third component.***

Figure 8a shows the first component (PC1) which is the one encloses the maximum variability of the system. The second component (PC2) exhibits some absorption of energy towards the left of the figure. The third component (PC3) shows a greater level of energy absorption to the left of a figure indicating that presumably iron oxides specimens may be deposited towards that side.

In an effort to try to identify some of the mineral specimens in the Escondida district, it will be interesting to look into some characteristics of the spectral signatures of some typical specimens. Figure 9 shows some typical spectral signatures of minerals.

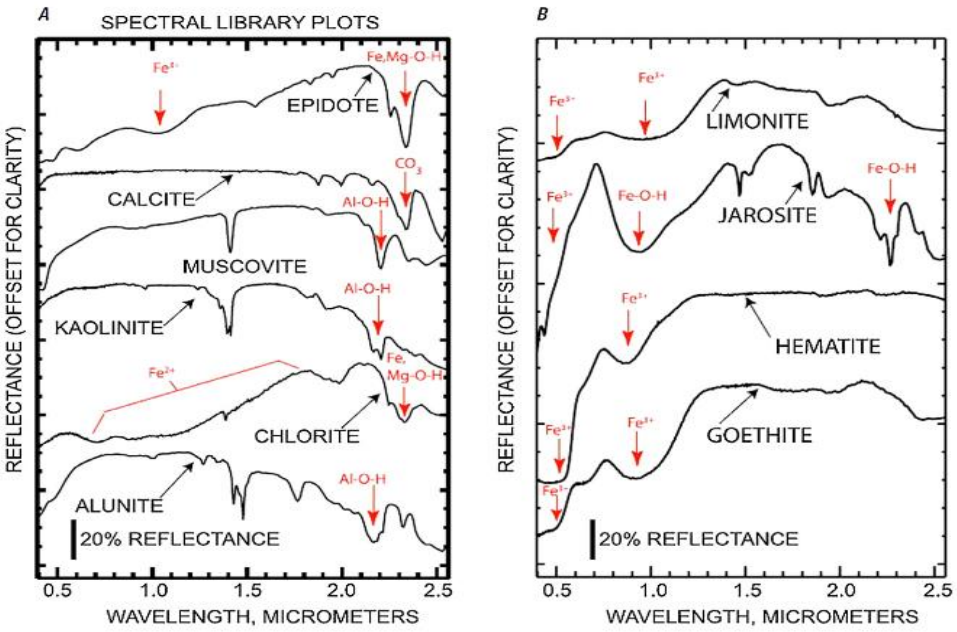


***Fig. 9 (A) Laboratory spectra of epidote, calcite, muscovite, kaolinite, chlorite and alunite. (B) Laboratory spectra of limonite, jarosite, hematite and goethite (Clark et al., 1993) mentioned by A. B. Pour (2015)***

As noted in Figure 9, the spectral signatures of different elements are viewed along the complete wavelength space in a general continuous displacement but, from time to time, they produce a sort of "***jumps***" to lower (or to higher) and then to higher (or to lower) values or vice-versa. For instance, in Figure 9 (A) muscovite, kaolinite, and alunite decay around wavelength 1.4-1.6 μm; they also decay around 2.1-2.3 μm. In Landsat-8 it means that these three specimens, decay along the wavelength neighborhoods in accord to ***band 6 and band 7***. In the same fashion, in Figure 9 (B) specimens such as limonite, jarosite, hematite, and goethite decay around 0.5– 0.65 μm and 0.80-0.90 μm and also in the interval 0.85-0.88 μm and 1.6–1.7 μm. These intervals´ neighborhoods correspond to ***band 2*** and ***band 4***, and ***band 5*** and ***band 6.*** On the other hand, Figure 10 describes the spectral signatures of olivine and pyroxene specimens as well as plagioclase feldspar at a level of laboratory. In this case, decays are produced in the wavelength intervals 1.1 and 2.5 μm .

The relevance of the eigenvalues and their sign – positive/negative - is for being the factor which impact the original DN values of an image to get a new DN associated with the bands of each Principal Component (PC) to obtain an image for this PC at each of the pixels.

In regard to this, ***Gupta, R.P et al*** (2013) refer to "…. *a method called "feature oriented principal components selection" (FPCS). In this, they selectively used only those spectral bands for PC analysis which would have relevance for particular mineral discrimination and identification. They tested its effectiveness in detecting spectral anomalies due to ferric iron oxide minerals." He adds "This technique has been applied by many workers for mapping alteration minerals using PCA".*

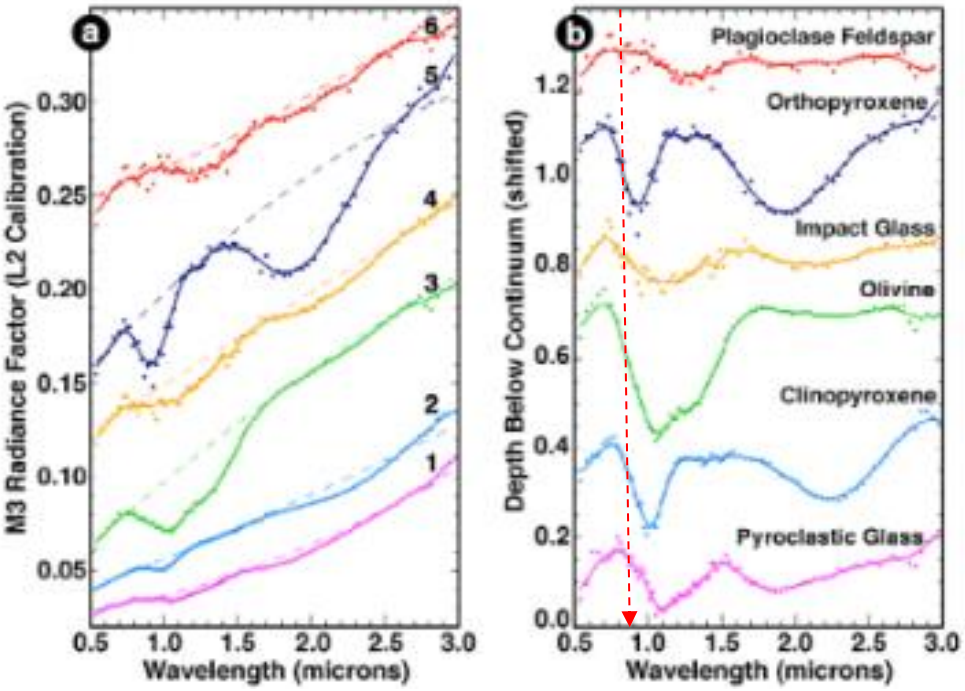


***Figure 10. Reflectance and wavelength (μm) for olivine, pyroxene, and plagioclas feldspar minerals (B. Horgan et al, 2014).***

| Band contrast | Wavelength range (μm) | Comment *(B. Horgan, 2014)* |
|---|---|---|
| **B2**<br>**B4** | **0.452 0.512**<br>**0.636 0.673** | ***goethite, hematite, magnetite,….***<br>***Figure 10 (b)*** |
| **B5**<br>**B6** | **0.851 0.879**<br>**1.567 1.651** | ***goethite, hematite, magnetite,….***<br>***Figure 10 (b)***<br>***olivine, pyroxenes, others*** *(Le Hung Trinh, 2016.). Also B. Horgan et al, 2014.* |
| **B6**<br>**B7** | **1.567 1.651**<br>**2.107 2.294** | ***alunite, illite, kaolinite, chlorite***<br>***Figure 10 (a)*** |

Table 3 Summary relations of distinctive wavelength intervals of the electromagnetic spectrum associated with the presence of hydrothermal altered mineral specimens.

Table 1, which has numerical data associated with the different Landsat-8 bands should give us some insights regarding mineral identification. As a matter of fact, some other workers have showed (***W.P. Loughlin, 1991***) that in altered hydrothermal deposits it is more interesting to look for the differences in patterns affecting the whole eigenvector-eigenvalue matrix than to focus on the first three principal components. Several applications have been conducted using the same argument (***A. Crosta et al, 1989; W.P. Loughlin, 1991; D.Aydal et al, 2007; A. Crosta et al, 2003***), that is, to look for contrasting enhancements in the eigevector-eigenvalue matrix to improve the presence of specific objects in the scene: the purpose being to stand out the brightness difference between pixels and their backgrounds.

To consider the eigenvector-eigenvalues of the PCA matrix for visualization purposes it is essential to recognize both the "high/low broken wavelength interval" and their magnitudes. In Figure 11 it can be noticed that the greater discrepancies between contrasting eigenvalue loadings along the seven bands are in components 4 (bands 5-6-7), 5 (bands 3-4-5-6), and 6 (2-3-4-5-6). Component 2 includes values very similar to each other (Table 1); component 3 (Figure 12) shows also some brightness discrepancies but at a level of magnitudes much lower than the 4, 5, and 6 components.

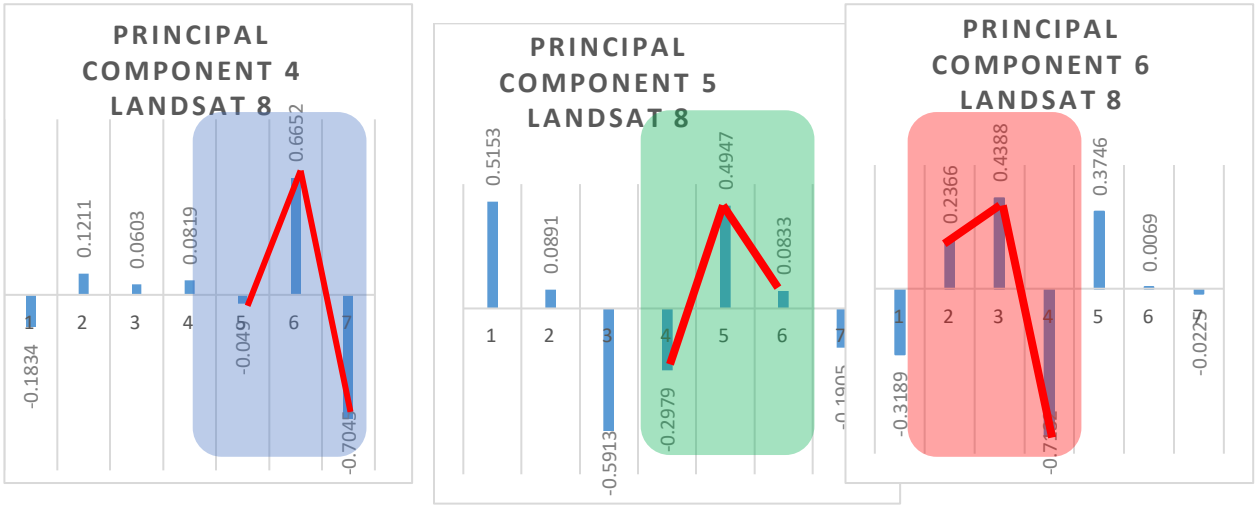


***Figure 11. Principal Components Landsat-8 showing the eigenvalues distribution along the seven bands. Major discrepancies (high and low values from one band to its neighbors) in pixel brightness are concentrated in components 4, 5, and 6.***

Because the level of contrasting eigenvalue data is sufficiently representative of the PCA dealing with Landsat 8, they will be used for visualization of the image captured by this satellite.

The same exercise has been done to analyze the Sentinel 2 data.

| | PC1 | PC2 | PC3 | PC4 | PC5 | PC6 | PC7 |
|---|---|---|---|---|---|---|---|
| B1 | 0.3151 | 0.6376 | -0.0127 | -0.1591 | 0.0584 | -0.0924 | 0.6312 |
| B2 | 0.3147 | 0.6272 | -0.0410 | 0.1701 | -0.0116 | 0.0908 | -0.6372 |
| B3 | 0.3176 | -0.1406 | 0.2955 | -0.4648 | -0.6820 | -0.2548 | 0.0967 |
| B4 | 0.3171 | -0.1463 | 0.1561 | 0.0165 | 0.1079 | -0.4875 | -0.0149 |
| B5 | 0.3167 | -0.1491 | 0.2171 | 0.0714 | 0.2211 | -0.2426 | -0.1006 |
| B6 | 0.3163 | -0.1524 | 0.1828 | 0.0560 | 0.3411 | 0.0299 | -0.1548 |
| B7 | 0.3167 | -0.1514 | 0.1491 | -0.0641 | -0.5571 | 0.6774 | -0.0185 |

Table 4. Principal Components Matrix with Eigenvalue Loadings Sentinel 2 on the Escondida district

The explained variance has been concentrated, in practice, only in the first component which shows very similar values for all the band set.

| Eigenvalues | Explained variance | Cumulative variance |
|---|---|---|
| **6.558450** | **99.072999** | **99.072999** |
| **0.055650** | **0.840671** | **99.913671** |
| 0.0045482 | 0.0687061 | 99.982377 |
| 0.0006479 | 0.0097876 | 99.992164 |
| 0.0002363 | 0.0035704 | 99.995735 |
| 0.0001606 | 0.0024263 | 99.998161 |
| 7.4864948 | 0.0011309 | 99.999292 |

Table 5 Eigenvalues and explained variance – PCA Sentinel-2 – Escondida district

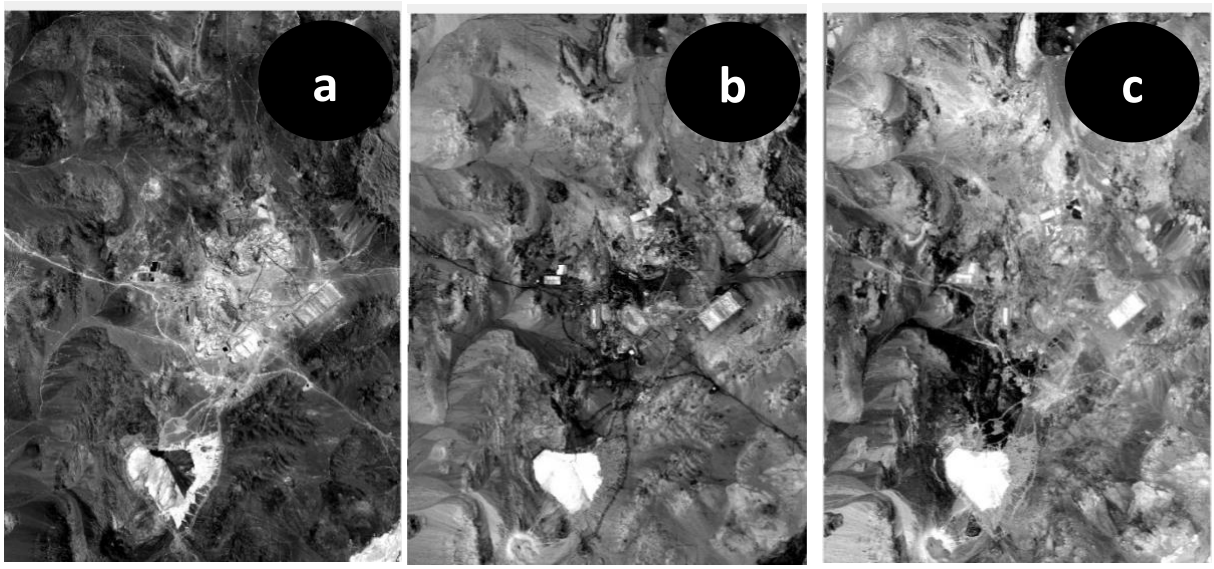


***Figure 12. Visualizations of the first three Components in the PCA analysis on the Escondida district using Sentinel-2. (a) first component; (b) second component; (c) third component.***

Comments on Figure 13 are similar to those regarding Figure 8. Insufficient for any type of minerals identification.

To determine the most convenient components to visualize the Escondida on the basis of Sentinel-2, the same procedure employed in the case of Landsat-8 will be applied.

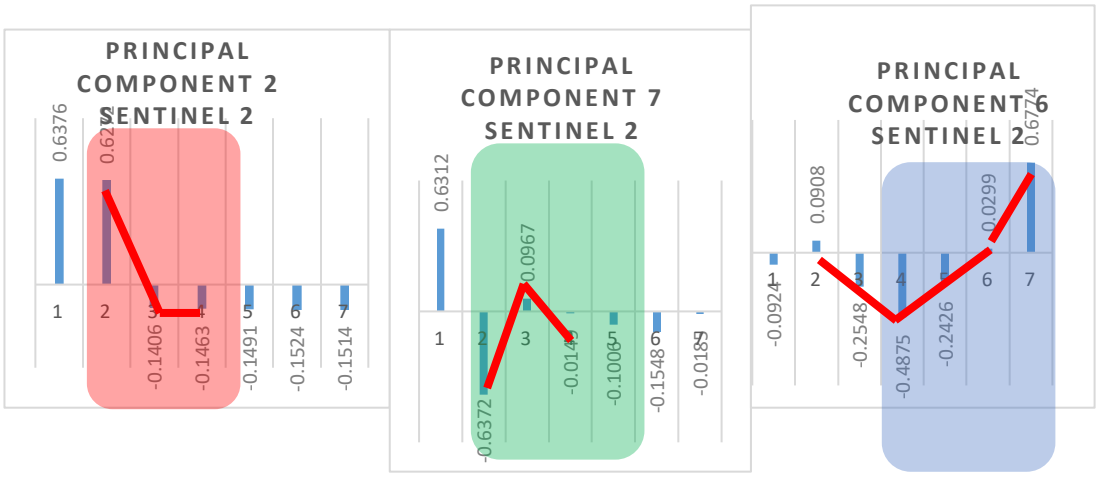


***Figure 13. Principal Component Sentinel-2 showing the eigenvalue loadings with the "high & low" values across the wavelength spectrum indicating the transition from energy brightness to energy absorption.***

In summary:

Landsat-8 and Sentinel-2 satellites have shown on Escondida short-spectral-signature intervals along the wavelength spectra associated with some selected components of the eigenvector-eigenvalue matrix. Table 6 shows the summary

| **Landsat-8** | | **Sentinel-2** | |
|---|---|---|---|
| Components | **Bands** | Components | **Bands** |
| 4 | (5)-6- 7 | 2 | 2-(3)-4 |
| 5 | (4)-5- 6 | 7 | 2-(3)-4 |
| 6 | 2–(3)-4 | 6 | 5-6-7 |
| Summary | B2-B4 /B6-B5 / B6-B7 | Summary | B2–B4 /B5-B6/B6-B7 |

Table 6. Summary of the bands´ interrelations that, based on distinctive components, define short-intervals of the wavelength spectra where the presence of selected minerals is detected.

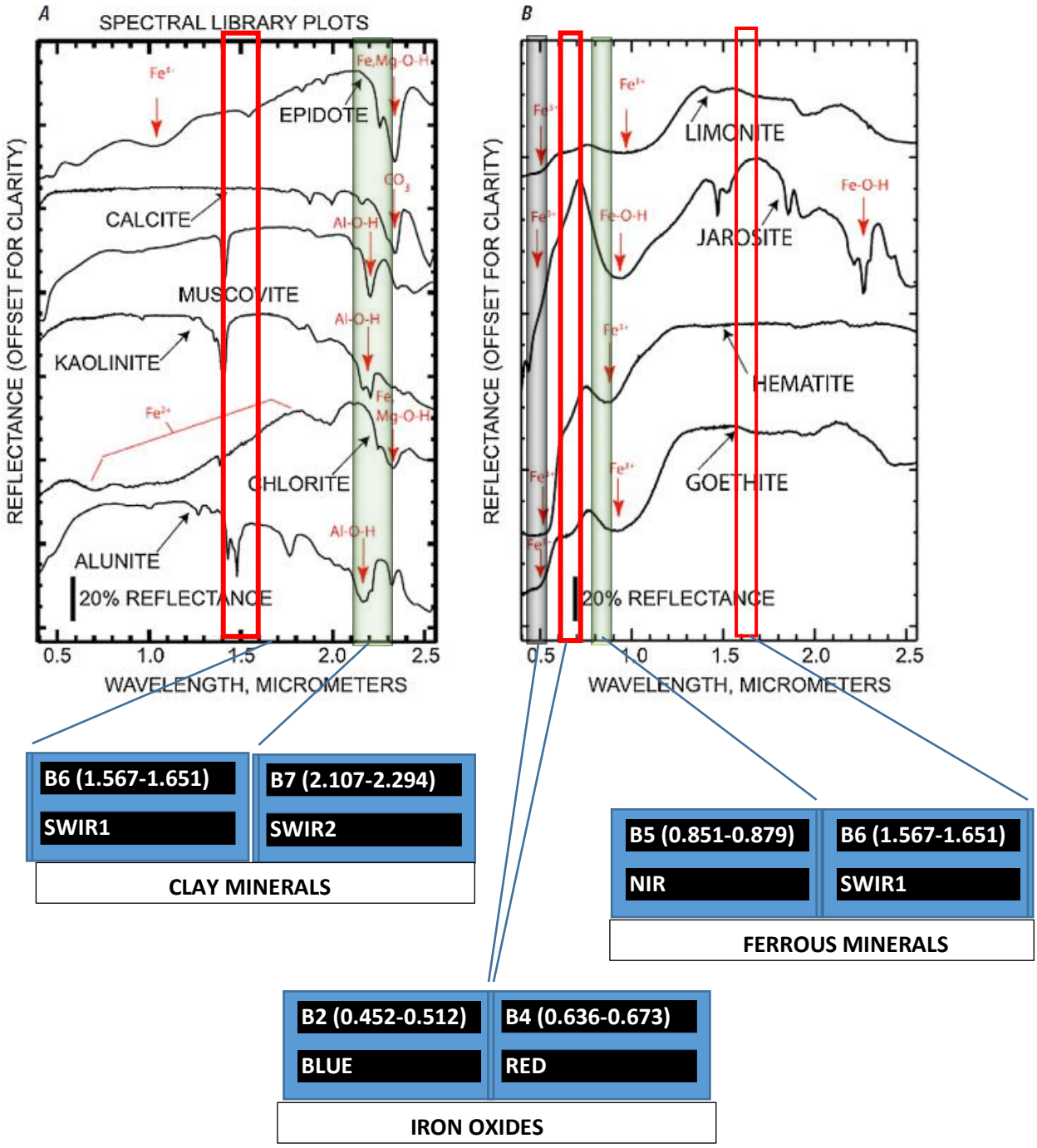


***Figure 14. Wavelength-intervals where iron oxides (hematite, magnetite, and others), ferrous minerals (olivine, pyroxenes, others), clay minerals (alunite, chlorite, kaolinite, and others) are detected in Escondida through the PCA analysis using Landsat-8 and Sentinel-2 satellites.***

.

PCA analysis has been used in this thesis to try to approach mine site visualization and corroboration of minerals specimens.

## Mine site visualization

Visualization has been addressed in two ways:

(1) Through the ***first three Principal Components*** of the PCA analysis using the Landsat-8 and the Sentinel-2, Figures 8 and 13. Both triad of figures are very similar to each other showing, with special quality, the ground topography. Discrimination of different geological structures is difficult, or almost impossible, without having any field work.

(2) Through the selection of ***components 4-5-6 in the case of Landsat-8*** and ***2-7-6 in the case of Sentinel-2*** and their relations between eigenvalues data and associated bands, identification of distinctive wavelength intervals have corroborated the presence of selected minerals specimens dealing with iron oxides, ferrous minerals, and clay minerals as Table 6 shows

As a matter of fact, the geological map of Figure 15 (Below) shows most of the key minerals available in the district. Specimens, as most of the hydrothermally altered deposits, are in line with the minerals indicated in the text of Figure 14.

Figure 15 shows the visualization of the Escondida district using the components 4-5-6 of a PCA analysis in the case of Land-8 and the components 2-7-6 of a PCA analysis in the case of Sentinel-2 as well as the geological map referred above. Map has been done based on outcrops in the mine-site and interpreted in accordance with various geological teams.

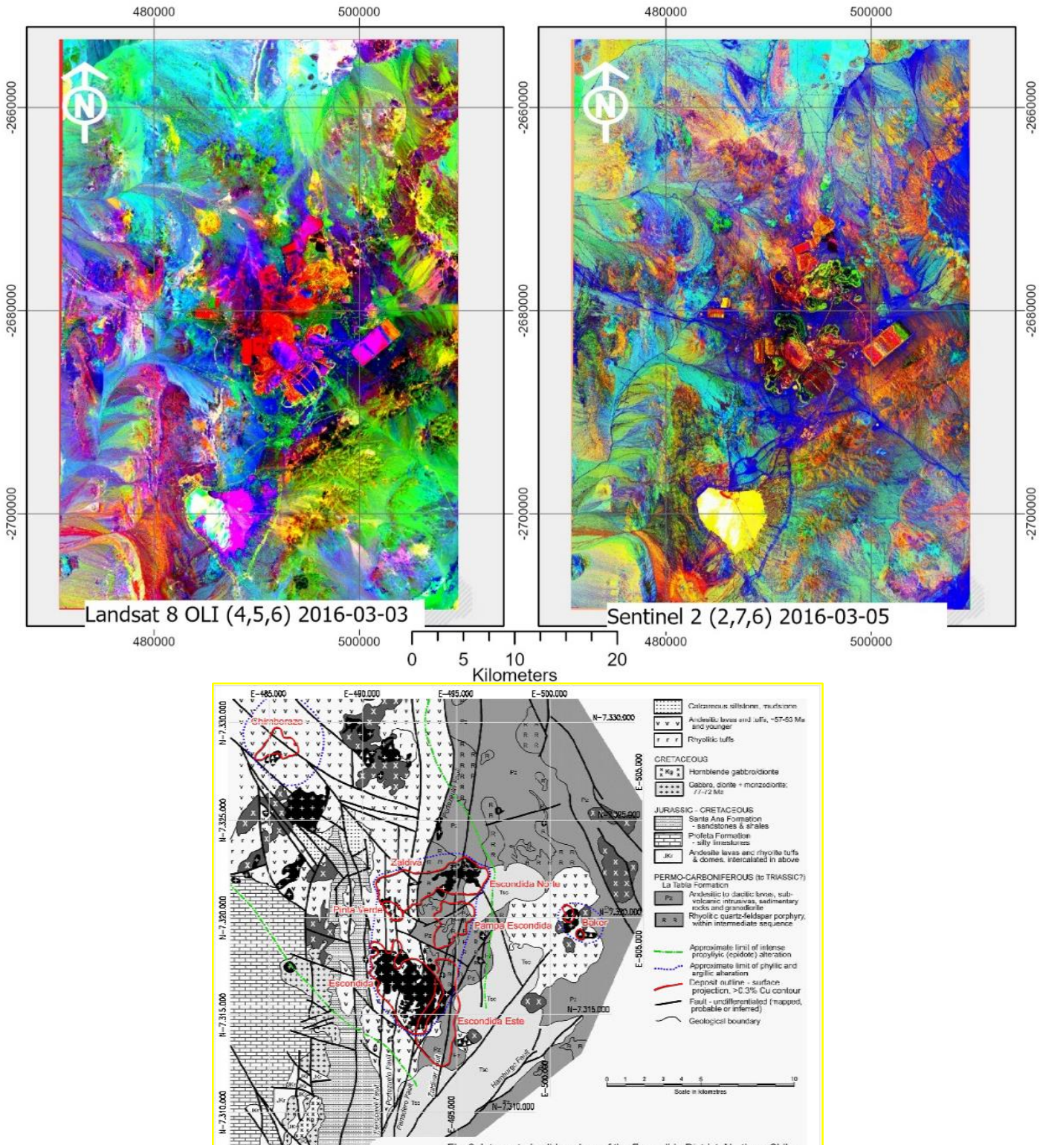


***Figure 15. (Above, left) Visualization of the Escondida district using Landsat-8 and components 4, 5, 6 of a PCA analysis. (Above, right) Visualization of the Escondida district using Sentinel-2 and components 2, 7, 6 of a PCA analysis. (Below) Map of Escondida district (Figure 2).***

Based on the previous analysis as well as in the interest for the characterization of mineral specimens, it is necessary now to set up a series of spectral signatures allowing a better identification of those specimens. To perform this identification and estimation on a very specific site, this procedure will be carried out within the area of the argillic alteration which is the final phase of mineralization..

Literature review provide various spectral indices in geology (***Z. Ourhzif et al, 2019; A.F. Alasta, 2011; D. Segal, 1982; S. Drury, 1990).***

Based on those suggestions and in the analysis under way, eight ratios were considered for analysis:

| | | | | | | | |
|---|---|---|---|---|---|---|---|
| 4/2 | 4/7 | 5/4 | 6/2 | 6/5 | 6/7 | 7/2 | 7/6 |

Table 7. Series of band ratios for identification and measurement of mineral specimen occurrences

The ratio 4/2 is useful for mapping iron oxides because it has absorption in the blue region, where it has a high reflectance in the red region. The ratio 6/7 has the ability to map some clay minerals such as kaolinite, montmorillonite. The ratio 6/5 has been used for mapping ferrous minerals due to the high reflectance of these minerals in this ratio (***R. Gupta, 2003***).

Band ratios derived from image spectra (4/2, 6/7, 5/4 in RGB) is used for the identification of argillic alteration´s mineral specimens.

Finally, for geological classification using Landsat-8 the following platform was set up:

| | | | | | |
|---|---|---|---|---|---|
| 4/2 | 6/5 | 6/7 | 5/4 | PC 2 | PC 6 |

Table 8. Series of band ratios for classification of mineral specimen occurrences --- Landsat 8

For the geological classification using Sentinel-2 the following platform was set up:

| | | | | | |
|---|---|---|---|---|---|
| 4/2 | 11/8a | 11/12 | 8a/4 | PC 2 | PC 6 |

Table 9. Series of band ratios for classification of mineral specimen occurrences --- Sentinel 2

Below, Figure 16, shows the extensions of iron oxides within the argillic alteration zone of Escondida in accord with Landsat-8 and Sentinel-2.

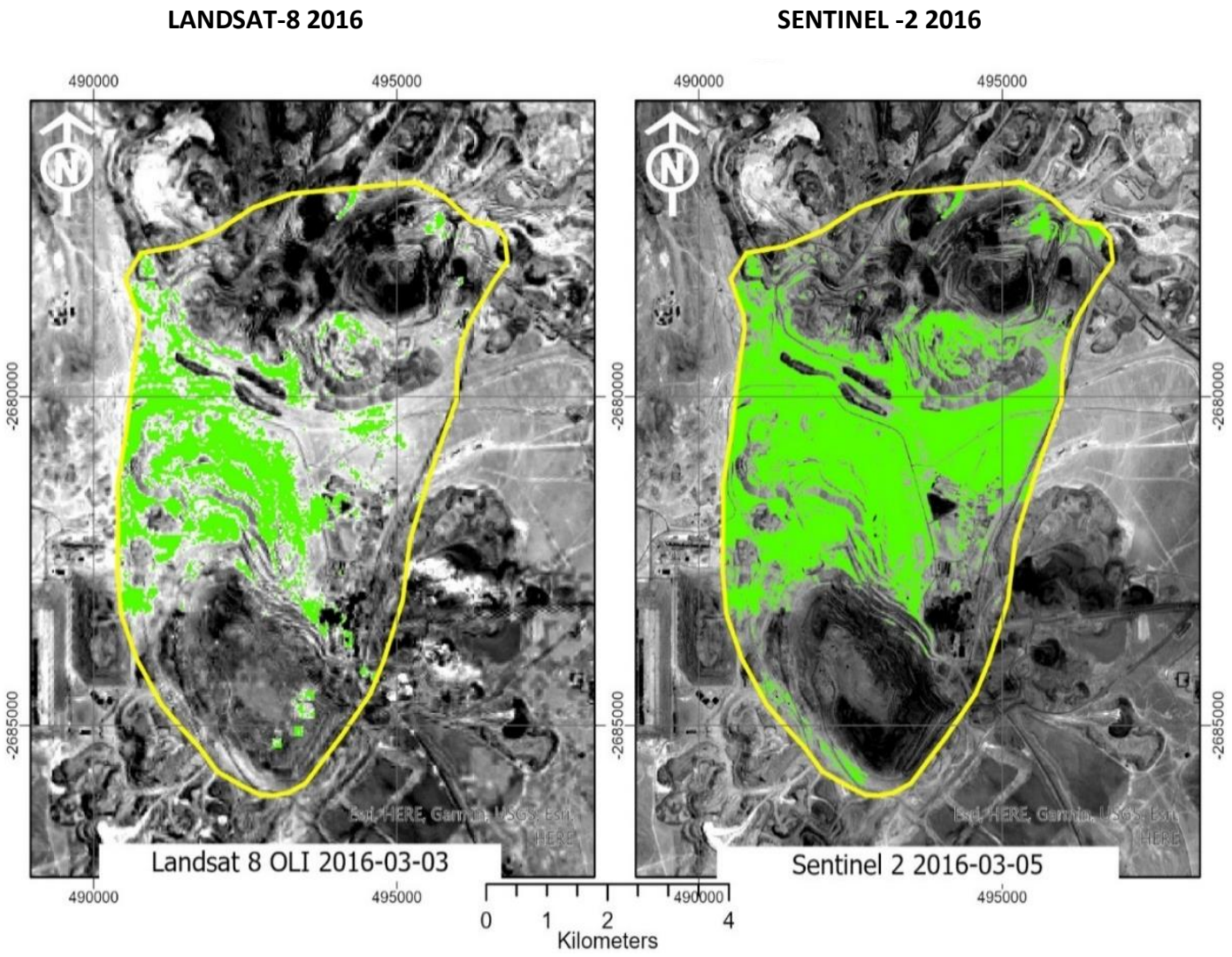


***Figure 16. B4/B2 for (a) Landsat-8 and (b) Sentinel-2´s Geological extensions of Iron Oxides in Escondida 's argillic alterations***

Index B4/B2 is suitable for detecting the presence of iron oxides such as limonite, hematite, goethite along with K-feldespar. Sentinel-2 shows a better contrast when using this index. Similar situations are displayed using index B6/B5 (or B11/B8a) for detecting clay minerals), and index B6/B7 (or B11/B12) for detecting ferrous minerals.

**LANDSAT-8 2016** **SENTINEL -2 2016**

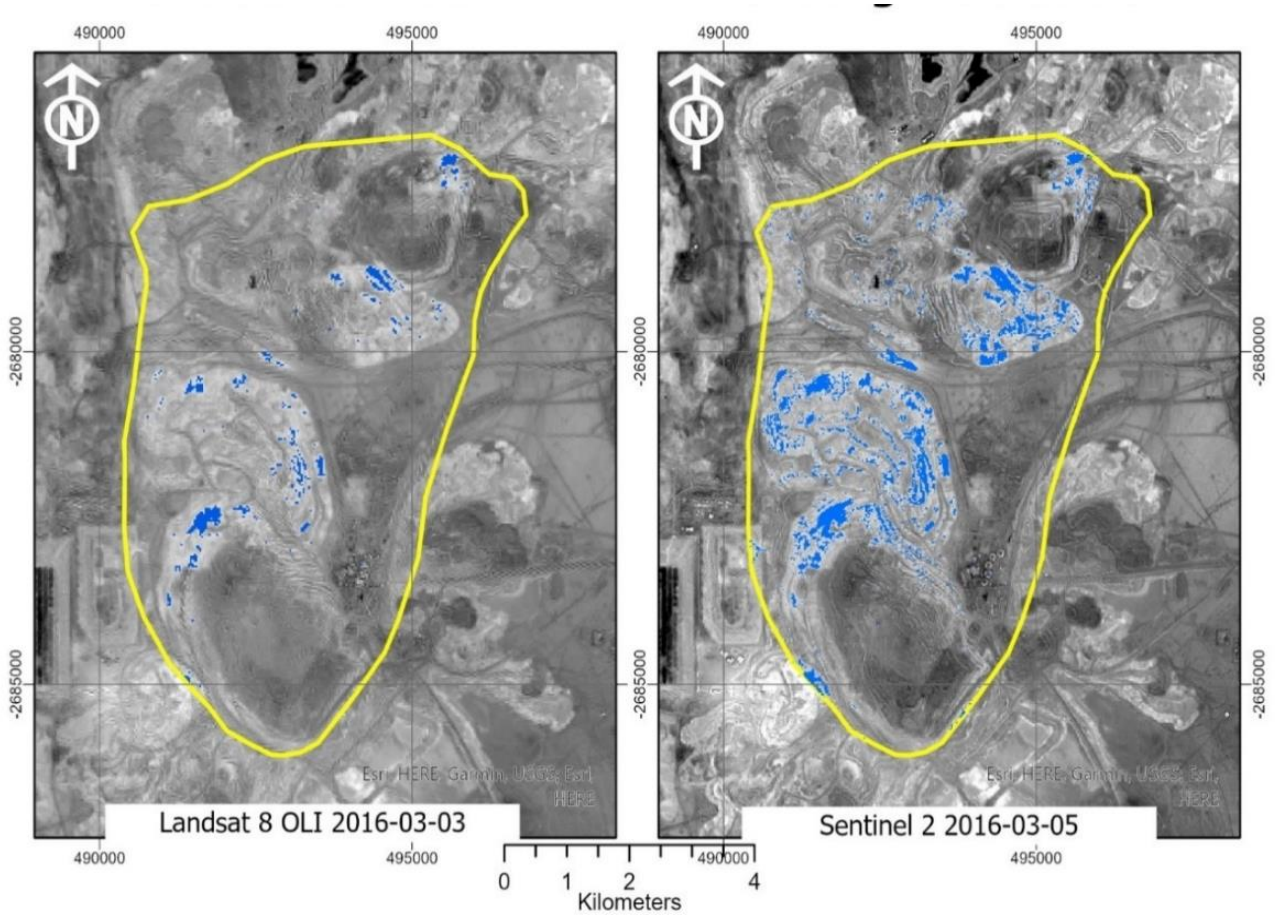


***Figure 17. (a) B6/B5 for Landsat-8 and (b) B11/B8a for Sentinel-2. Geological visualization of ferrous minerals in Escondida´s argillic alteration***

**LANDSAT-8 2016** **SENTINEL -2 2016**

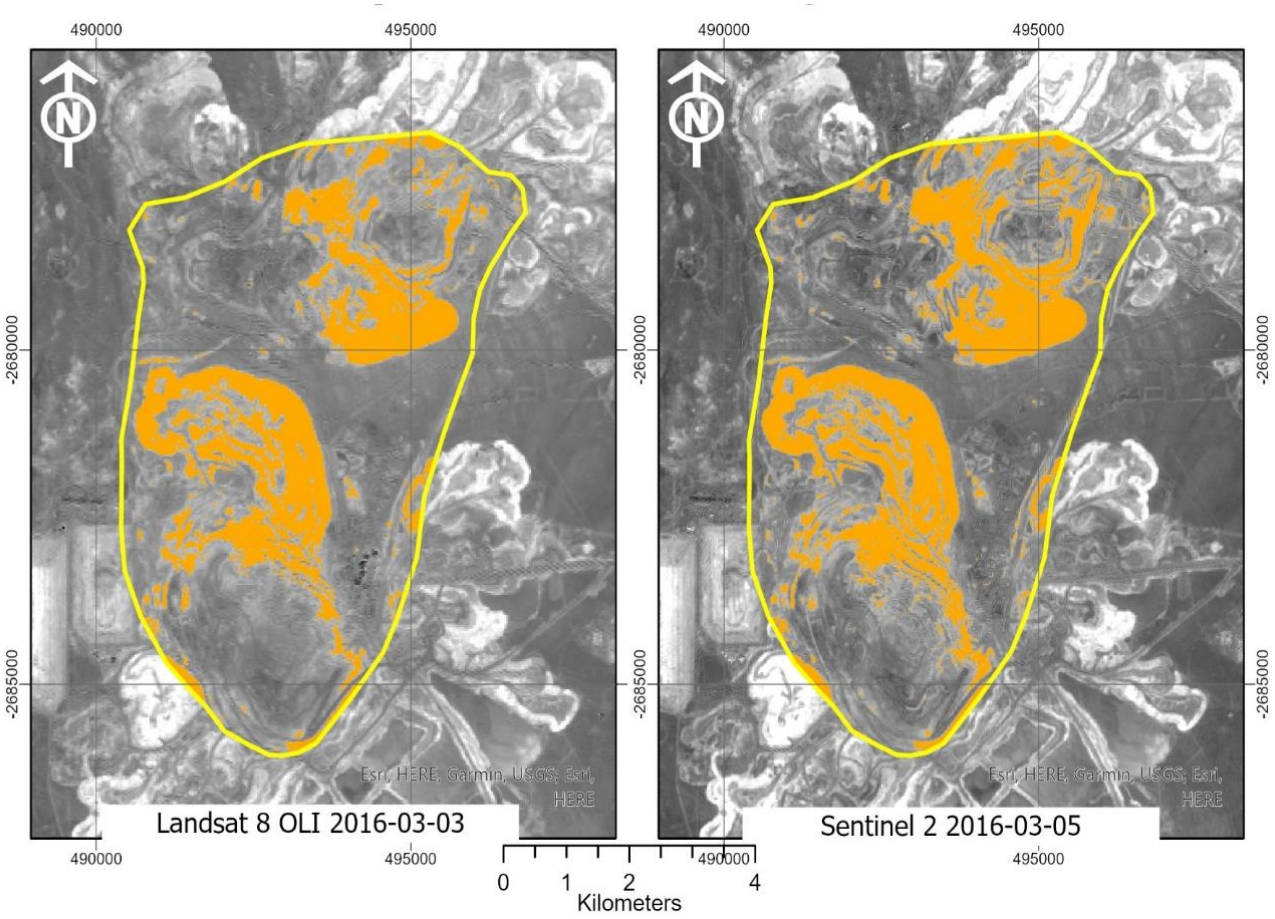


***Figure 18. (a) B6/B7 for Landsat-8 and (b) B11/B12 for Sentinel-2. Geological extensions of clay in Escondida´s argillic alteration***

In the present study, the Landsat 8 bands 4, 5, 6, and 7 are highly effective in discriminating various rock units. Various rock units such as quartz feldspathic schist rocks shown by white pixels and igneous and metamorphic rocks exhibit by dark pixels can be easily discriminated. High reflectance correspond to band 6; low reflectance corresponds to band 5. The ratio 6/7 has the ability to map kaolinite, montmorillonita and clay minerals. *(Z. Ourhzif et al 2019).*

As a summary, within the argillic alteration sector (4,114 Ha) in Escondida, the extensions of these three groups of minerals follows:

As a complementary information, and according to mineral processing studies, there is a 12% of Kaolinite, a 4% of montmorillonite, and a 18% of Illita in the Escondida mine (*Bulatovic et al, 1999*).

| MINERAL OCCURRENCES | Extension (Ha); % of alteration zone on the basis of Landsat-8 | Extension (Ha); % of alteration zone on the basis of Sentinel-2 |
|---|---|---|
| | | |
| IRON OXIDES | 621,5 (15,11%) | 1,330,0 (32,32%) |
| FERROUS MINERALS | 56,2 (1,36%) | 223,1 (5,42%) |
| CLAY | 866,0 (21,05%) | 978,5 (23,78%) |

Table 10. Areal extensions of Iron Oxides, Ferrous Minerals, and Clay Minerals at Escondida ´s superficial argillic alteration zone (4,114Ha)

## 3.4 Classification

In Appendix, classification procedures have been divided in supervised, unsupervised, and object-based methodology. In this case, a supervised procedure was applied using for this a classification software (an algorithm or classifier based on machine learning) to perform the classification activity. Four ratios (red/blue, swir1/nir, swir2/swir1 and nir/red), and two components (PC2, and PC6) were chosen for image generation.

Following, twenty classes within the image available were considered but, after analyzing the whole scene the focus was ***on one specific occurrence in the surrounding neighborhood of the two main pits at Escondida***. Samples were chosen for the due training on the target specimen and a group of fifty secondary samples were considered to assess their matching on the target specimen. A Random Tree classifier was employed for this analysis and results are given in Figure 19, Figure 20, and Table 11.

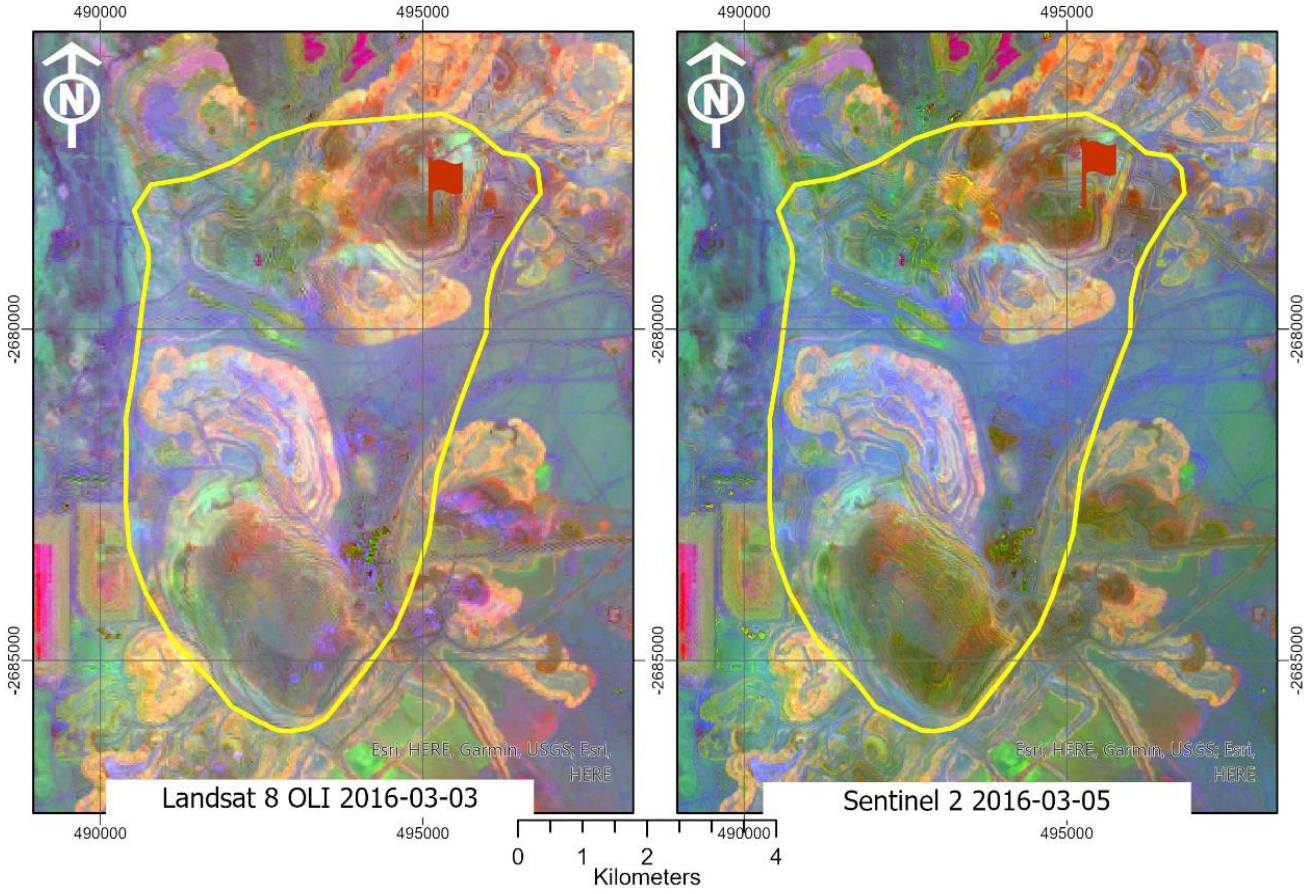


Figure 19 Identified Mineral Target Occurrences
within Escondida superficial argillic alteration zone (4,114 Ha)

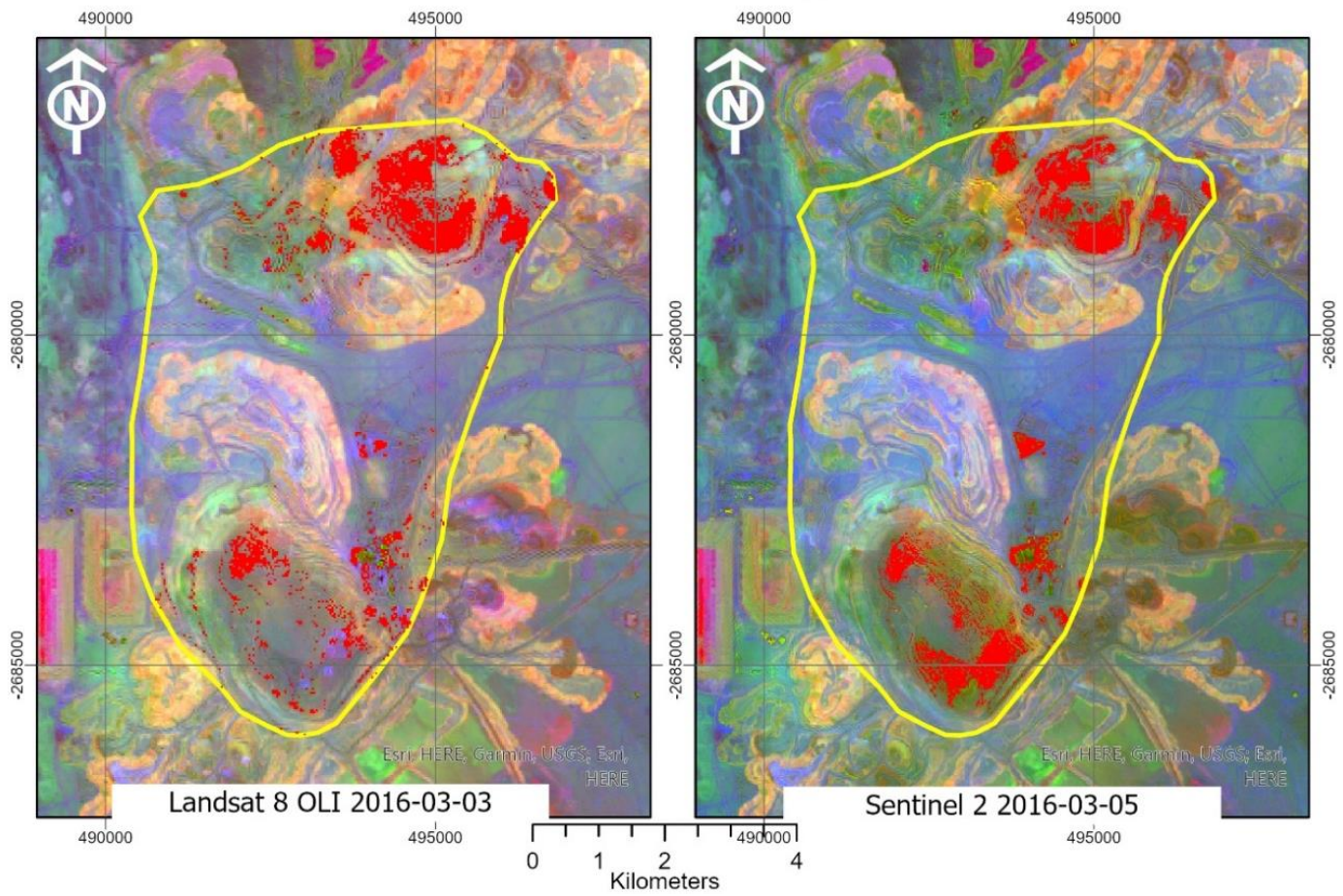


Figure 20 Classified Mineral Target Occurrences
within Escondida superficial argillic alteration zone (4114 Ha)

| **LANDSAT-8** | **SENTINEL-2** |
|---|---|
| ***295 Ha*** | ***321 Ha*** |

Table 11 Classified Target Extension

## 3.5 Assessment of Classified Target Mineral Occurrences

The assessment of classified target mineral occurrences was done by using confusion matrices.

| CLASSES | TARGET | OTHER | TOTAL | ACCURACY | KAPPA |
|---|---|---|---|---|---|
| TARGET | 23 | 2 | 25 | 0.92 | 0 |
| OTHER | 5 | 20 | 25 | 0.80 | 0 |
| TOTAL | 28 | 22 | 50 | 0 | 0 |
| Paccuracy | 0.8214 | 0.9090 | 0 | 0.86 | 0 |
| | | | | | 0.72 |

Table 12 Confusion Matrix for Landsat -8

| CLASSES | TARGET | OTHER | TOTAL | ACCURACY | KAPPA |
|---|---|---|---|---|---|
| TARGET | 24 | 1 | 25 | 0.96 | 0 |
| OTHER | 7 | 18 | 25 | 0.72 | 0 |
| TOTAL | 31 | 19 | 50 | 0 | 0 |
| Paccuracy | 0.7741 | 0.9473 | 0 | 0.84 | 0 |
| | | | | | 0.68 |

Table 13 Confusion Matrix for Sentinel 2

## 4. Discussion

- ***On the Sentinel-2 capability for mineral exploration in arid regions***.

  Through this investigation it is clear that Sentinel-2 performs remote sensing processes in mineral exploration with similar efficiency and effectiveness that Landsat-8. Band composition, band ratios, PCA analysis, spectral indices, and classification procedures have been applied under which, Landsat-8 and Sentinel-2 have performed in agreement with the objectives established. There was only one noticeable difference between the results of Landsat-8 and Sentinel-2: the estimation of the minerals extensions. Although all comparisons between Landsat-8 and Sentinel- 2 were consistently under the same parameters and conditions, the difference in extension among them can be a result of the different statistical values considered in each case by the software. It should be interesting to prove Sentinel-2 over land with bushes and thick vegetation to evaluate its limitations.

- ***On products obtained as results***

  Among the products obtained as results Sentinel-2 has provided similar results than Landsat-8 in

  - illustrating images for geological distinction at large scale (**band composition**)
  - visualizing the mine-sites using a **PCA** analysis through (a) the components enclosing the maximum variabilities (first three components); (b) components selected through contrasting positive/negative eigenvalue-loadings associated with the bands sequence.
  - identifying and measuring the typical groups of mineral in hydrothermally altered copper-molybdenum deposits through **band ratios**.
  - classifying target mineral occurrences through a **supervised classification technique** including the "random trees" classifier as a machine learning algorithm.
  - **assessing a sampling procedure** within the classification process on the basis of a confusion matrix.

- ***On exploration data***

  It is interesting to notice that the most important group of minerals in a hydrothermally altered deposit is the iron oxide minerals family (32%) following by the clay minerals (23%). Ferrous minerals reach only 5%.

- ***On the assessment of classification***

  In terms of the classification done on Escondida´ argillic alteration area, the assessment index is both cases are almost similar between Landsat- 8 an Sentinel-2 (72% and 68% respectively) which are classified at a "*good*" level according to the standards in remote sensing**.**

## 5. Conclusions

Although results could have been much more complete and the interpretation of the images much more convincing, remote sensing is an activity than can add substantially more value to mineral exploration. This because remote sensing is a relatively inexpensive activity in comparison to other mineral exploration activities, it can quickly generate maps of large exploration areas, and it can obtain images of any area of interest. It is evident that a good skill in the interpretation of images is necessary.

In this work only an interpreted geological map has been used. With field work and data on sampling, geological structures, exclusive mineral pathfinders, and more results would had improved notably.

**At ending this work I would like to respond to the three questions posed at the very beginning of it:**

**How Sentinel-2 applications & procedures match landsat-8 ones**

***Sentinel-2 applicability & activities in remote sensing match very well those used by landsat-8 considered this as a reference technology.***

**How Sentinel-2 spatial resolution impact remote sensing results**

***Sentinel-2 spatial resolution impact in benefit of a better discrimination of some elements such as structural and geological features for mineral exploration providing a satisfactory definition of a geological environment and a suitable discrimination of their mineralization border's which is of utmost importance in mineral exploration.***

**How we can improve the results of the analysis for mining exploration using remote sensing?**

***Definitively remote sensing alone is not enough for mineral exploration. It offers a good sense of what kind of minerals could be under or over surface. To improve the results more than a geologic map is required. Data such as geochemical sampling, geophysics data, a few rock samples and hopefully some field work, would presumably improve notoriously the results.***

# 6. Bibliography


**Aydal,D et al** *Application of the Crosta technique for alteration mapping of granitoidic rocks using ETM+ data: case study from eastern Tauride belt (SE Turkey), International Journal of Remote Sensing, 28:17, 3895-3913, DOI: 10.1080/01431160601105926, 2007.*

**Alasta, Amro F.** *Using Remote Sensing data to identify iron deposits in central western Libya. International Conference on Emerging Trends in Computer and Image Processing (ICETCIP'2011) Bangkok Dec., 2011.*

**Biswajit, N. et al** *Observation of short-term variations in the clay minerals ratio after the 2015 Chile great earthquake (8.3 Mw) Using Landsat 8 OLI Data; May 2019; Journal of Earth System Science July 2019,(128:117):1-21; DOI: 10.1007/s12040-019-1129-2*

**Borie, C. et al** *Beyond Site Detection: The Role of Satellite Remote Sensing in Analyzing Archaeological Problems. A Case Study in Lithic Resource Procurement in the Atacama Desert, Northern Chile, MDPI, Remote Sens. 2019, 11, 869; doi:10.3390/rs11070869 www.mdpi.com/ journal/ remote sensing*

**Bulatovic, S. et al** *Effect of clay slimes on copper, molybdenum Flotation from porphyry ores, in Proceedings of the Copper 99-Cober 99 International Conference, 95-111, Phoenix, 1999.*

**Crosta A.** *Targeting key alteration minerals in epithermal deposits in Patagonia, Argentina, using ASTER imagery and principal component analysis INT. J. REMOTE SENSING, 10 NOVEMBER, 2003, VOL. 24, NO. 21, 4233–4240*

**Crosta, A. and J. McM.Moore** *Enhancement of Landsat ThematicMapper Imagery for Residual Soil Mapping in SW Minais Gerais State, Brazil: A Prospecting Case History in Greenstone Belt Terrain. Proceedings of the 7th (ERIM) Thematic Conference: Remote Sensing for Geology. Calgary, 2-6 Oct,1989 pp: 1173- 1187.*

**Ducart, D.F. et al** *Mapping iron oxides with Landsat-8/OLI and EO 1/Hyperion imagery from the Serra Norte iron deposits in the Carajás Mineral Province, Brazil Brazilian Journal of Geology, 46(3): 331-349, September 2016*

**Delgadillo-Herrera, M. et al** *Normalized difference indices in Landsat 5 TM satellite data. Proceedings Volume 11104. Current Developments in Lens Design and Optical Engineering XX; 111040W: 2019 https://doi.org/10.1117: 12:2532322*

**Di Tommaso, I et al** *Hydrothermal Alteration Mapping Using ASTER Data in the Infiernillo Porphyry Deposit, Argentina. Ore Geology Reviews, 32, 275-290, 2007. http://dx.doi.org/10.1016/j.oregeorev.2006.05.004*

**Drury, S. A.** *A Guide to Remote Sensing: interpreting images of the Earth. Oxford University Press,1990*

**El Atillah, A. et al** *Use of the Sentinel-2A Multispectral Image for Litho-Structural and Alteration Mapping in Al Glo'a Map Sheet (1/50,000) (Bou Azzer–El Graara Inlier, Central Anti-Atlas, Morocco), 2019*

**Gandhi, S et al** *Essentials of Mineral Exploration and Evaluation Paperback ISBN: 9780128053294; eBook ISBN, 2016:9780128053324.*

**Gupta, R.P.** *Gupta, R.P. (2003) Remote Sensing Geology. 3rd Edition, Springer-Verlag, Berlin, 655. http://dx.doi.org/10.1007/978-3-662-05283-9, 2003*

**Gupta, R.P. et al** *A Simplified Approach for Interpreting Principal Component Images Advances in Remote Sensing, 2013, 2, 111-119 http://dx.doi.org/10.4236/ars.2013.22015 Published Online June 2013 (http://www.scirp.org/journal/ars)*

**Hervé, M et al** *Geologic Overview of the Escondida Porphyry Copper District, Northern Chile: in Society of Economic Geologists, Special Publication 16, pp. 55-78.*

**Horgan, Briony . et al** *Near-infrared spectra of ferrous mineral mixtures and methods for their identification in planetary surface spectra, ICARUS, 234 (214) 132-154; 2014*

**Horning, N.** *Selecting the appropriate band combination for an RGB image using Landsat imagery, Center for Biodiversity and Conservation, 2004*

**Horning, N.** *Understanding pixels, bands and channels, Version 1.0 (2004). American Museum of Natural History, Center for Biodiversity and Conservation. Available from http://biodiversity informatics.amnh.org. (accessed on date)*

**Jaadi, Z.** *A Step-by-Step Explanation of Principal Component Analysis (PCA), Built-in, 2021*

**Kim, J-C et al** *Application of Landsat images to Snow Cover Changes by Volcanic Activities at Mt. Villarrica and Mt. Llaima, Chile; Korean Journal of Remote Sensing, Vol.30, No.3, 2014, pp.341~350 http://dx.doi.org/10.7780/kjrs.2014.30.3.1*

**Loughlin, W.P.** *Principal Component Analysis for Alteration Mapping; Photogrammetric Engineering & Remote Sensing, Vol. 57, No. 9, September 1991, pp. 1163-1169. 0099-1112'9V5709-1163$03.00/0 Q1991 American Society for Photogrammetry and Remote Sensing*

**Monna, F. et al** *Tracking archaeological and historical mines using mineral prospectivity mapping; Journal of Archaeological Science journal homepage: 49-2014 (57- 69) http://www.elsevier.com/locate/ja*

**NASA 13** *NASA's 2013 Year in Review https://www.nasa.gov*

**NASA 11** *NASA's 2013 Year in Review https://www.nasa.gov*

**Noble, W.S.** *What is a support vector machine? Nature Publishing Group http://www.nature.com/nature-biotechnology Computational Biology PRIMER, 2006*

**Ott, N et al** *GIS analyses and favorability mapping of optimized satellite data in northern Chile to improve exploration for copper mineral deposits , Geosphere 2(4): 236-252 , 2006*

**Ourhzif, Z. et al** *Lithological Mapping using Landsat 8 OLI and Aster Multispectral Data in Imini-ounilla District South High Atlas of Marrakech; The International Archives of the Photogrametry, Remote Sensing and Spatial Information Sciences, Volume XLII-2/W13, 2019 ISPRS Geospatial Week 2019, 10-14 June 2019, Enschede, The Netherland*

**Pizarro, A. et al** *Geology and Discovery of Escondida Este Porphyry Cu-Mo Deposit, Escondida Cluster District, Northern Chile: in Geologia Economica y Recursos Naturales, Exploracion Andina, Neuvos Hallazgos y Actializaciones, XIV Congreso Geologica Chilena, Las Serena, October, 2015, Proceedings v.2, pp. 382-384.*

**Pour, B et al** *Using spectral mapping techniques on short wave infrared bands of ASTER remote sensing data for alteration mineral mapping in SE Iran International Journal of the Physical Sciences Vol. 6(4), pp. 917-929, 18 February, 2011 Available online at http://www.academicjournals.org/IJPS DOI: 10.5897/IJPS10.510 ISSN 1992 - 1950 ©2011 Academic Journals*

**Porter Geo Data** *Escondida - Escondida Norte, Escondida Este, Zaldivar, Pinta Verde, Pampa Escondida, Chimborazo, Baker, Pamela, Rincones*

**Rux, N.** *ESRI, https: // storymaps. arcgis. com*

**Richards, J. A. et al** *Remote sensing digital image analysis: An introduction. Berlin Springer Verlag; 2006.*

**Richards, J.P. et al** *Geologic evolution of the Escondida Area, Northern Chile model for spatial and temporal localization of Porphyry Mineralization: in Econ. Geol. v96 pp 271-305*

**Rockwell, B.W. et al.** *Identification of quartz and carbonate minerals across northern Nevada using ASTER thermal infrared emissivity data—Implications for geologic mapping and mineral resource investigations in well-studied and frontier areas, Geosphere 4(1), 2008, DOI: 10.1130/GES00126.1*

**Sabins, F.** *Remote Sensing; Ore Geology Review Volume 14, Issues 3–4, September 1999, Pages 157-183*

**Segal, D** *Theoretical Basis for Differentiation of Ferric-Iron Bearing Minerals, Using Landsat MSS Data. "Proceedings of Symposium for Remote Sensing of Environment, 2nd Thematic Conference on Remote Sensing for Exploratory Geology, Fort Worth, TX (1982): pp. 949-951.*

**Vincent, R.K** **Fundamentals of Geological and Environmental Remote Sensing.** *Prentice Hall Series in Geographic Information Science xiii + 370 pp. Hemel Hempstead: Prentice Hall. ISBN 0 13 348780 6*

**Wenyan, G et al** *Assessment of the Capability of Sentinel-2 Imagery for Iron-Bearing Minerals Mapping: A Case Study in the Cuprite Area, Nevada, Remote Sensing 12(18):16;2020.*

**Wob Editions** *Fundamentals of Geological and Environmental Remote Sensing, 2022, Prentice Hall Series, 2022*

**Yazdi, M. et al** *Landsat ETM+ imaging for mineral potential mapping: Application to Avaj area, Qazvin, Iran; International Journal of Remote Sensing · August 2013*

**Yazdi, M. et al** *Landsat ETM+ imaging for mineral potential Mapping application to Avaj area, Qazvin, Iran, International Journal of Remote Sensing and Remote Sensing Letters 2012*

**Yiu, T.** *Understanding Random Forest, Remote Sensing Tutorials N.M. Short, 1999* ***http://drr.ikcest.org/remotesensing.tutorial/front/collab.html*** *Toward Data Science 2019*

**Zakaria, J.** *A Step-by-Step Explanation of Principal Component Analysis (PCA)] Builtin.com/data science/ April 1, 2021*

# APPENDIX

**Remote Sensing basic review**

## Remote Sensing basic review

***NOTE:*** ***In this Appendix, a compilation of papers, documentations, and internet links are presented. Citations are all indicated.***

Remote sensing is the technology that captures information about the Earth's surface without actually being in contact with it. This is done because different objects reflect or emit different amounts of energy in different bands of the electromagnetic spectrum (***John A. Richards, 2012***). The amount of energy reflected or emitted depends on the properties of both the material and the incident energy (angle of incidence, intensity and wavelength). Detection and discrimination of objects or surface features is done through the uniqueness of the reflected or emitted electromagnetic radiation from the object. A device to detect this reflected or emitted electro-magnetic radiation from an object is called a "sensor" (e.g., cameras and scanners). A vehicle used to carry the sensor is called a "platform" (e.g., aircrafts and satellites); Figure 1.

Main stages in remote sensing (***N. Rux, ESRI, https: // storymaps. arcgis. com***) are the following:

(a) Emission of electromagnetic radiation
(b) The Sun or an electro-magnetic-radiation (EMR) source located on the platform B and transmission of this energy from the source to the object
(c) Absorption and scattering of the EMR while transmission
(d) Interaction of EMR with the object and subsequent reflection and emission
(e) Transmission of energy from the object to the sensor
(f) Recording of energy by the sensor
(g) Photographic or non-photographic sensors
(h) Transmission of the recorded information to the ground station
(i) Processing of the data into digital or hard copy image
(j) Analysis of data.

These stages (***R.K. Vincent, 2022; S.M. Gandhi et at, 2016***) are shown in Figure 1.

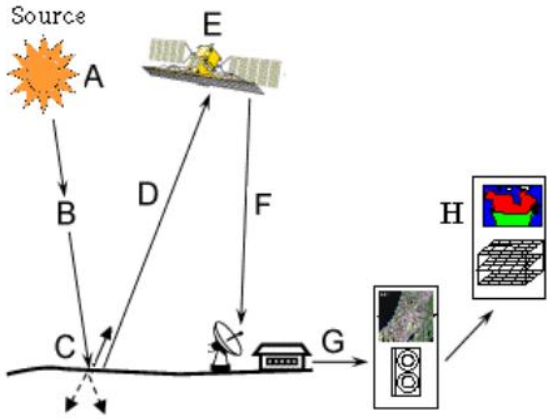


*Figure 1. Stages in remote sensing*

## Sensors

There exist at present a variety of sensor space-crafts (Aster, World View, SPOT, Ikaros, and many others). However, our interest is in two of them: Landsat-8 and Sentinel-2. Both provide satellite images without any payment; all the other sensors charge for providing satellite images.

As the link ***https://landsat.gsfc.nasa.gov/satellites/ landsat-8/*** describes, the "*Landsat-8 satellite is an American Earth observation satellite launched on 11 February 2013 It is the eighth satellite in the Landsat program; the seventh to reach orbit successfully. Originally called the Landsat Data Continuity Mission (LDCM), it is a collaboration between NASA and the United States Geological Survey (USGS). NASA Goddard Space Flight Center in Greenbelt, Maryland, provided development, mission systems engineering, and acquisition of the launch vehicle while the USGS provided for development of the ground systems and will conduct on-going mission operations. It comprises the camera of the Operational Land Imager (OLI) with 30m spatial resolution and nine bands, and the Thermal Infrared Sensor (TIRS) with 100m spatial resolution and two bands which can be used to study Earth surface temperature and is used to study global warming.*

*The satellite was built by Orbital Sciences Corporation, who served as prime contractor for the mission. The spacecraft's instruments were constructed by Ball Aerospace & Technologies and NASA's Goddard Space Flight Center (GSFC), and its launch was contracted to United Launch Alliance (ULA). During the first 108 days in orbit, LDCM underwent checkout and verification by NASA and on 30 May 2013 operations were transferred from NASA to the USGS when LDCM was officially renamed to Landsat 8. The area covered by each scene is 185 × 180 km*".

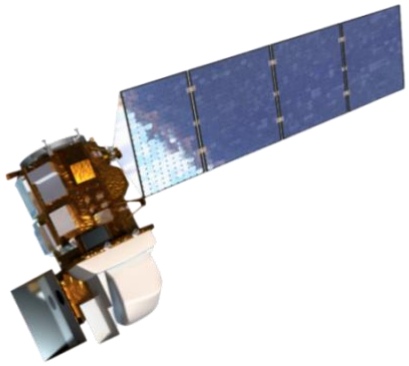

*Figure 2. The Landsat-8 space-craft*

In a parallel fashion, the link ***https://www.esa.int/Applications/ Observing the Earth/ Copernicus/Sentinel-2*** describes the Copernicus Sentinel-2 mission S2/MSI as "*a mission with two satellites (S2A/MSI and S2B/MSI launched by the European Union's Copernicus Earth Observation program of Europe Space Agency (ESA) in 2015 and 2017, respectively). Both S2 satellites carry the Multi-Spectral Instrument (MSI), a sensor containing 13 bands and spatial resolution varying between 10 and 60 m at visible to shortwave infrared (SWIR) regions Because of their spectral capabilities (including three bands in the Red-edge and two bands in the SWIR), S2/MSI mission provides new mapping possibilities. It aims at monitoring variability in land surface conditions, and its wide swath width (290 km) and high revisit time (10 days at the equator with one satellite, and 5 days with 2 satellites under cloud-free conditions which results in 2-3 days at mid-latitudes) will support monitoring of Earth's surface changes*"

A similar link ***https://sentinels.copernicus.eu/web/sentinel/missions/sentinel-2/satellite*** complements the previous information adding that "*the Sentinel-2 satellite system was developed by an industrial consortium led by Astrium GmbH (Germany). Astrium SAS (France) is responsible for the MultiSpectral Instrument (MSI). The MSI works passively, by collecting sunlight reflected from the Earth. New data is acquired at the instrument as the satellite moves along its orbital path*".

"*The incoming light beam is split at a filter and focused onto two separate focal plane assemblies within the instrument; one for Visible and Near-Infra-Red (VNIR) bands and one for Short Wave Infra-Red (SWIR) bands. The spectral separation of accomplished by stripe filters mounted on top of the detectors*".

*Figure 3. The Sentinel-2 space-craft*

Wavelengths as well as their mid-points (CW) are calculated differently for Landsat 8 and Sentinel-2 - see below for description, Figure 4 *(GIS Ag Maps.com)*.

| L8 Band | | CW (µm) | Wavelength (lower-upper) | Bandwidth | Res. (m) | | S2 Band | | CW (µm) | Wavelength (min-max) | Bandwidth | Res. (m) |
|---|---|---|---|---|---|---|---|---|---|---|---|---|
| 1 | C/A | 0.443 | 0.435 - 0.451 | 0.016 | 30 | C/A | 1 | C/A | 0.443 | 0.421 - 0.457 | 0.036 | 60 |
| 2 | Blue | 0.482 | 0.452 - 0.512 | 0.060 | 30 | Blue | 2 | Blue | 0.494 | 0.439 - 0.535 | 0.096 | 10 |
| 3 | Green | 0.561 | 0.533 - 0.590 | 0.057 | 30 | Green | 3 | Green | 0.560 | 0.537 - 0.582 | 0.045 | 10 |
| 4 | Red | 0.655 | 0.636 - 0.673 | 0.037 | 30 | Red | 4 | Red | 0.665 | 0.646 - 0.685 | 0.039 | 10 |
| | | | | | | | 5 | VRE | 0.704 | 0.694 - 0.714 | 0.020 | 20 |
| | | | | | | | 6 | VRE | 0.740 | 0.731 - 0.749 | 0.018 | 20 |
| | | | | | | | 7 | VRE | 0.781 | 0.768 - 0.796 | 0.028 | 20 |
| | | | | | | | 8 | NIR | 0.834 | 0.767 - 0.908 | 0.141 | 10 |
| 5 | NIR | 0.865 | 0.851 - 0.879 | 0.028 | 30 | NIR | 8a | NIR | 0.864 | 0.848 - 0.881 | 0.033 | 20 |
| | | | | | | | 9 | WV | 0.944 | 0.931 - 0.958 | 0.027 | 60 |
| 9 | Cirrus | 1.373 | 1.363 - 1.384 | 0.020 | 30 | Cirrus | 10 | Cirrus | 1.375 | 1.338 - 1.414 | 0.076 | 60 |
| 6 | SWIR | 1.609 | 1.567 - 1.651 | 0.085 | 30 | SWIR | 11 | SWIR | 1.612 | 1.539 - 1.681 | 0.142 | 20 |
| 7 | SWIR | 2.201 | 2.107 - 2.294 | 0.187 | 30 | SWIR | 12 | SWIR | 2.194 | 2.072 - 2.312 | 0.240 | 20 |
| 8 | Pan | 0.590 | 0.503 - 0.676 | 0.172 | 15 | | | | | | | |
| 10 | TIRS | 10.895 | 10.60 - 11.19 | 0.590 | 100 * | | | | | | | |
| 11 | TIRS | 12.005 | 11.50 - 12.51 | 1.010 | 100 * | | | | | | | |

*Figure 4. Central wavelength, wavelength range, bandwidth, Resolution Comparison between Landsat 8 and Sentinel 2 (GIS Ag Maps.com)*

▪

As described in ***https://www.quora.com; https://romgistors.blogspot.com/2015/05/brief-introduction-to-remote-sensing.html***, **Sensors** "*can be on board of airplanes or on board of satellites, measuring the electromagnetic* ***radiation at specific ranges*** *(usually called* ***bands****). If the source of the measured energy is the Sun, then it is called passive remote sensing, and the result of this measurement can be a* ***digital image****. If the measured energy is not emitted by the Sun but from the sensor platform then it is defined as active remote sensing, such as radar sensors which work in the microwave range (****Richards and Jia, 2006****). The range of energy examined in a remote sensing system is broken into 256 bins. A single pixel may have several* ***digital number*** *(DN) variables corresponding to different bands recorded".*

An image is made up of individual elements that are arranged in a grid of rows and columns. These elements are called ***pixels***. In fact, the word "pixel" is derived from "picture element". As a result, the measures are quantized and converted into a ***digital image***, where each picture elements (i.e. pixel) has a discrete value in units of Digital Number, DN (*NASA, 2013*). The resulting images have different characteristics (resolutions) depending on the sensor. There are several kinds of resolutions:

**Spatial resolution**, as ***https://fromgistors.blogspot.com*** *defines it* usually measured in pixel size, "*is the resolving power of an instrument needed for the discrimination of features and is based on detector size, focal length, and sensor altitude"; spatial resolution is also referred to as geometric resolution or IFOV;*

**Spectral resolution**, in accord with ***https://www.earthdatascience.org/courses/earth-analytics/multispectral-remote-sensing-data/introduction-multispectral-imagery-r/***, "*is the number and location in the electromagnetic spectrum (defined by two wavelength indices) of the spectral bands in multispectral sensors, for each band corresponds an image; Such as Figure 5 shows, theoretically, the electromagnetic radiation extends along the whole wavelength spectrum as a sequence of adjacent ranges called* ***bands****. Space-crafts captures, according to the nature of each of them, radiations from only privilege bands within the whole wavelength spectrum",* Figure 6. Expressions of the spectral signatures along these selective bands support the configuration of the spectral signature of an object/material.

A whole spectrum of radiation is shown in Figure 5.

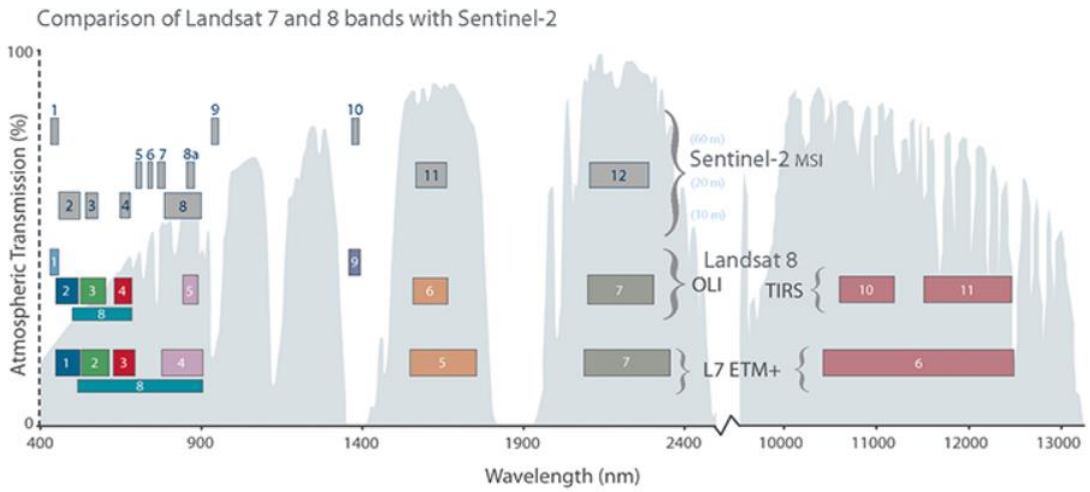


*Figure 5. The electromagnetic spectrum*
*(Earth Resources Observation and Science (EROS) Center March 1, 2019)*

**Radiometric resolution**, as defined in ***https://semiautomaticclassificationmanual-v5.readthedocs.io/ru/latest/remote_sensing.html*** **,** ***"****usually measured in bits (binary digits), is the range of available brightness values, which in the image correspond to the maximum range of DNs; for example, an image with 8-bit resolution has 256 levels of brightness"* (*Richards and Jia, 2006*);

For satellites sensors, there is also the *temporal resolution*, which is the time required for revisiting the same area of the Earth.

Other definitions follow:

## Radiance and Reflectance

Sensors, in agreement with ***https://semiautomaticclassificationmanual-v5.readthedocs.io/fa/latest/remote_sensing.html****, measure the radiance, which corresponds to the brightness in a given direction toward the sensor; it is also useful to define the reflectance as the ratio of reflected versus total power energy. Images in radiance can be converted to Top of Atmosphere (TOA) Reflectance (combined surface and atmospheric reflectance) in order to reduce the in between-scene variability through a normalization for solar irradiance. The TOA reflectance becomes a unit-less ratio of reflected versus total power energy.*

## Spectral Signature

The link ***https://semiautomaticclassificationmanual-v5.readthedocs.io/de/latest/_remote_sensing.html*** also *defines the spectral signature as the reflectance as a function of*

*wavelength; each material has a unique signature, therefore it can be used for material classification. Remote sensing process **digital images** to extract **spectral signatures** at each **pixel** and use them to divide the image in groups of similar pixels (**segmentation**) using different approaches. As a last step, they assign a class to each group (**classification**) by comparing with known spectral signatures. Depending on pixel resolution, a pixel can represent many spectral signature "mixed" together - that is why much remote sensing analysis is done to "unmix" mixtures. Ultimately correct matching of spectral signature recorded by image pixel with spectral signature of existing elements leads to accurate classification in remote sensing.*

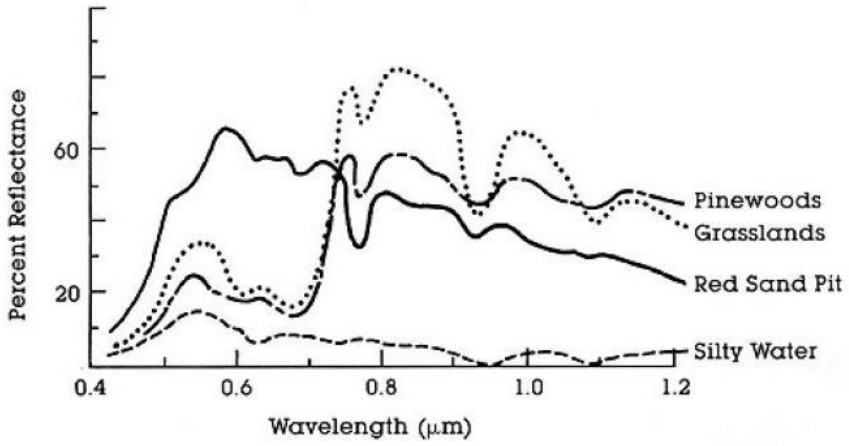


*Figure 6. Some spectral signatures*

*(NASA 2013)*

## Bands

***N. Horning (2004)*** comments that *a satellite image appears to be a 2-dimensional image. In reality, in addition to the rows and columns of pixels, images also have layers, or levels, also called "bands" which describe a range of wavelengths. They represent the different colors or light that are used to display an image on a computer screen*. These images are created on the basis of the three primary colors of light; red, green, and blue. The RGB primary colors can be mixed to create any color. By selecting three bands from a multi-band image and illuminating each of them with either red, green, or blue light we can create a color image, Figure 7. Another way to visualize this concept is to see how an individual pixel is composited. Figure 8 illustrates this same process for an individual pixel.

Below the Figure we see that a pixel has three layers; one each for the red, green, and blue light emitted from the computer screen. Each of these layers is represented by a number, the pixel value, which typically ranges from 0 - 255 where "0" represents black (no light) and

"255" represents very bright light. When each of these layers is illuminated by one of the primary colors of light, the color filter, and the layers are superimposed on top of one another, the appropriate color is produced for that pixel. If the pixel we want to view is from a black and white image we still use the three primary colors to create the image on the computer monitor. This is done by using the same pixel value for each of the pixel layers (***N. Horning, 2004***)

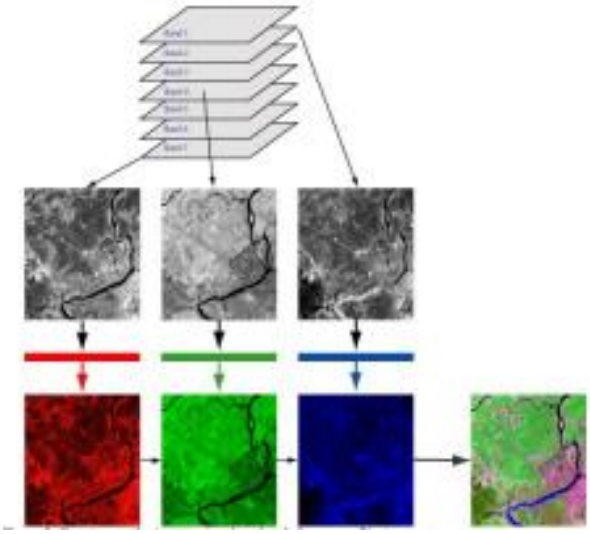

*Figure 7. Color image as a result of a RGB composite (N. Horning, version 1, 2004)*

To make a color image from images that have several bands we need to select three bands that can be assigned to the 3 color channels in a computer monitor, Figure 8.

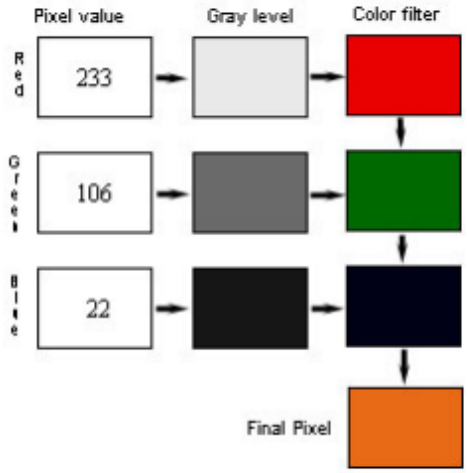


*Figure 8. Final Color Pixel Image*
*(N. Horning, version 1, 2004)*

## Band Ratios

Band Ratios are used to enhance the spectral differences between bands, as the link **https://www.L3harrisgeospatial.com/docs/bandratios.html** explains . Dividing one band (of high reflectance) by another (of high absorption) a process called "band ratio" allow us to enhance the spectral differences between bands whereby images providing relative band intensities are produced providing relative band intensities. The image enhances the spectral differences between bands. You may combine three ratios into a color-ratio-composite (CRC) image to determine the approximate spectral shape for each pixel's spectrum. Several band ratios are shown in the literature for mapping different minerals (***A. El Atillah et al, 2019***).

Band Ratio images improve the contrast between the features by partitioning the brightness values at ***peaks and troughs*** in a reflectance curve, after removing the atmospheric conditions from the image. Spectral band rationing enhances compositional information while suppressing other types of information about earth's surface. This method is very useful for highlighting certain features or materials that cannot be seen in the raw bands. Band ratio transformation is useful for qualitative detection of hydrothermal alteration minerals (***Di Tommaso. 2007; Rockwell et al. 2008; Pour, B. and Hashim, A. 2011***).

## PCA

Principal Component Analysis, or PCA, in accord with ***Z. Jaadi (2021)*** is a dimensionality-reduction method that is often used to reduce the dimensionality of large data sets, by transforming a large set of variables into a smaller one that still contains most of the information in the large set. PCA is a covered method on the web, and there are too many articles about it.

Principal component analysis can be broken down into five steps.

*a.* *Standardize the range of the continuous initial variables.* *The aim of this step is to normalize the range of the continuous initial variables so that each one of them contributes equally to the analysis. More specifically, the reason why it is critical to perform standardization prior to PCA, is that the latter is quite sensitive regarding the variances of the initial variables. That is, if there are large differences between the ranges of initial variables, those variables with larger ranges will dominate over those with small ranges. So, transforming the data to comparable scales can prevent this problem.*

**Z= (value - mean) / (standard deviation)**

*b.* *Once the standardization is done, all the variables will be transformed*

*c.* *to the same scale. The aim of this step is to understand how the variables of the input data set are varying from the mean with respect to each other, or in other words, to see if there is any relationship between them. This is done because, sometimes, variables are highly correlated in such a way that they contain redundant information. So, in order to identify these correlations, we compute the covariance matrix.*

*d.* *Compute the covariance matrix to identify correlations.*

*The covariance matrix is a* p × p *symmetric matrix (where* p *is the number of dimensions) that has as entries the covariances associated with all possible pairs of the initial variables. For example, for a 3-dimensional data set with 3 variables* x, y, *and* z, *the covariance matrix is a 3×3 matrix of this from:*

$$\begin{vmatrix} cov(x,x) & cov(x,y) & cov(x,z) \\ cov(y,x) & cov(y,y) & cov(y,z) \\ cov(z,x) & cov(z,y) & cov(z,z) \end{vmatrix}$$

*Since the covariance of a variable with itself is its variance (cov(a,a)=Var(a)), in the main diagonal (Top left to bottom right) we actually have the variances of each initial variable. And since the covariance is commutative (Cov(a,b)=Cov(b,a)), the entries of the covariance*

*matrix are symmetric with respect to the main diagonal, which means that the upper and the lower triangular portions are equal.*

*e. Compute the eigenvectors and eigenvalues of the covariance matrix to identify the principal components*

*f. Create a feature vector to decide which principal components to keep*

*7. Recast the data along the principal components axes*

PCA is done in order to reduce the number of variables of a data set. This naturally comes at the expense of accuracy, but the objective in dimensionality reduction is to trade a little accuracy for simplicity. Because smaller data sets are easier to explore and visualize and make analyzing data much easier and faster for machine learning algorithms without extraneous variables to process.

So to sum up, the idea of PCA is to reduce the number of variables of a data set, while preserving as much information as possible.

Eigenvectors and eigenvalues are the linear algebra concepts that we need to compute from the covariance matrix in order to determine the principal components of the data.

Principal components are new variables that are constructed as linear combinations or mixtures of the initial variables. These combinations are done in such a way that the new variables (i.e., principal components) are uncorrelated and most of the information within the initial variables is squeezed or compressed into the first components. So, the idea is N-dimensional data gives you N principal components, but PCA tries to put maximum possible information in the first component, then maximum remaining information in the second and so on.

Organizing information in principal components this way, will allow you to reduce dimensionality without losing much information, and this by discarding the components with low information and considering the remaining components as your new variables.

Geometrically speaking, principal components represent the directions of the data that explain a maximal amount of variance, that is to say, the lines that capture most information of the data. The relationship between variance and information here, is that, the larger the variance carried by a line, the larger the dispersion of the data points along it, and the larger the dispersion along a line, the more the information it has. In other words, principal components as new axes that provide the best angle to see and evaluate the data, so that the differences between the observations are better visible.

In regard to the eigenvectors and eigenvalues, they always come in pairs, so that every eigenvector has an eigenvalue. And their number is equal to the number of dimensions of the

data. For example, for a 3-dimensional data set, there are 3 variables, therefore there are 3 eigenvectors with 3 corresponding eigenvalues. Eigenvectors are the directions of the axes where there is the most variance (most information) and that we call Principal Components; and eigenvalues are simply the coefficients attached to eigenvectors, which give the amount of variance carried in each Principal Components.

## Classification

As the link *http://www.sc.chula.ac.th/courseware/2309507/Lecture/remote18.htm*e explains, “the intent of the classification process is to categorize all pixels in a digital image into one of several land cover classes, or "themes". This categorized data may then be used to produce thematic maps of the land cover present in an image. Normally, multispectral data are used to perform the classification and, indeed, the spectral pattern present within the data for each pixel is used as the numerical basis for categorization (Lilles and Kiefer, 1994). The objective of image classification is to identify and portray, as a unique gray level (or color), the features occurring in an image in terms of the object or type of land cover these features actually represent on the ground.

Two main classification methods are:

Supervised Classification and Unsupervised Classification.”

“With supervised classification, we identify examples of the Information classes (i.e., land cover type) of interest in the image. These are called "training sites". The image processing software system is then used to develop a statistical characterization of the reflectance for each information class. This stage is often called "signature analysis" and may involve developing a characterization as simple as the mean or the rage of reflectance on each bands, or as complex as detailed analyses of the mean, variances and covariance over all bands.”

Once a statistical characterization has been achieved for each information class, the image is then classified by examining the reflectance for each pixel and making a decision about which of the signatures it resembles most. (Eastman, 1995)”

Thus, digital image classification is the process of assigning a pixel (or groups of pixels) of a remote sensing image to a land cover class. The objective is to classify each pixel into only one class (crisp or hard classification) or to associate the pixel with many classes (soft classification). Because of my general familiarity with the mining industry, I applied a Supervised Classification.

**Reflectance and Bands along the Spectra Space**

As it was previously said, the emission and transmission of electromagnetic radiation from the Sun or from another platform with an electro-magnetic-radiation source to an object on the earth´s ground produces, after absorption and scattering of this radiation, the reflection of

it from the object to the platform and sensor which records the energy reflected. Each pixel responds in a very selected way to each band, sometimes a high reflectance is captured for a selected band, sometimes a very low reflectance is captured for another band. Sometimes the level of reflectance is very similar from band to band, other times there is significant contrast between the reflectance received by one band and the reflectance received by its neighbor band. As a result of this phenomenon, the reflected energy transmitted by any object in the ground is captured along the whole spectra, that is, along the whole wavelength space but showing, from time to time, "highs and lows" reflectance values. Figure 9 and Figure 10 explain this concept.

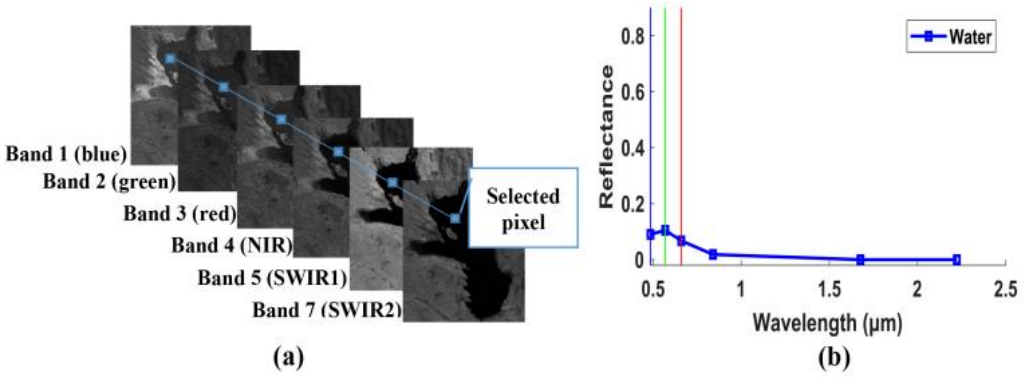


Figure 9. A one-water pixel selection

(a) in six spectral bands of Landsat 5 TM (b) spectral signature of the water pixel

(*M. Delgadillo-Herrera, et al, 2019*)

Six spectral bands(a) of Landsat 5 (***M. Delgadillo-Herrera et al, 2019***), converted into reflectance data (b) on one-pixel for display, Figure 9 and Figure 10..

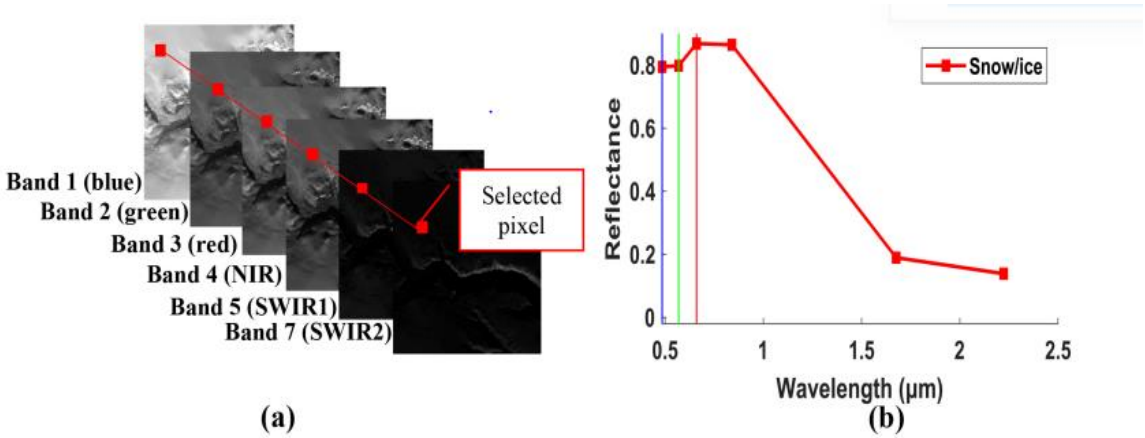


*Figure 10. A two-water/snow pixel selection*
(a) in six spectral bands of Landsat 5 TM (b) spectral signature of the snow/ice pixel
(*M. Delgadillo-Herrera, et al, 2019*)

It is very useful at this time to make reference to Band Mathematics (Band Math) (*https://www.l3harrisgeospatial.com/docs/bandmath.html*) which is a concept whereby different math operations can be developed to improve the visualization of land cover imaginary.

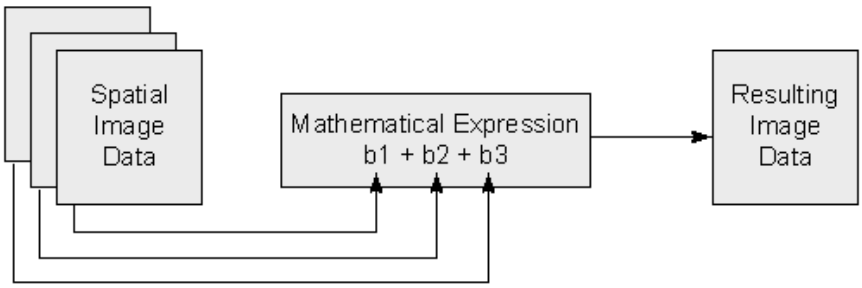


*Figure 11. A band math processing for an image data*
(*https://www.l3harrisgeospatial.com/docs/bandmath.html*)

**Reflectance, Bands, and Mineral Exploration**

Through time there have been several applications, experiences, and reports about the association existing between the energy reflected by some particular geological specimens and its capture by distinctive bands of the spectra space corresponding to different sensors.

(***A. El Atillah, 2019***). Bands or a combination of bands which privilege the visualization of some mineral specimens are usually called ***Spectral Geological Indices*** and they are applied for some specific group of minerals. For instance, we have:

## Clay Minerals Ratio

This band ratio highlights hydrothermally altered rocks containing clay and alunite. In the case of Landsat 8,

$$\text{Clay Minerals Ratio} = \frac{\text{SWIR1}}{\text{SWIR2}}$$

Where:

Shortwave-infrared (SWIR) 1: 1.567-1.651 µm
SWIR2: 2.107-2.294 µm
For Landsat 8, this corresponds to bands 6 (SWIR1) and 7 (SWIR2). This index works with any multispectral sensor with bands that fall within the listed ranges.

## Ferrous Minerals Ratio

This band ratio highlights iron-bearing minerals.

$$\text{Ferrous Minerals Ratio} = \frac{\text{SWIR1}}{\text{NIR}}$$

Where:

Shortwave-infrared (SWIR1) 1.567-1.651 µm
NIR: 0.851-0.879 µm
For Landsat 8, this corresponds to bands 6 (SWIR1) and 5 (NIR.SWIR2). This index works with any multispectral sensor with bands that fall within the listed ranges.

## Iron Oxide Ratio

This band ratio highlights hydrothermally altered rocks that have been subjected to oxidation of iron-bearing sulphides.

$$\text{Ferrous Minerals Ratio} = \frac{\text{Red}}{\text{Blue}}$$

Where:

Red: 0.636-0.673 µm
Blue: 0.452-0.512 µm

For Landsat 8, this corresponds to bands 4 (Red) and 2 (Blue). This index works with any multispectral sensor with bands that fall within the listed ranges

The ratio 4/2 is useful for mapping iron oxides because it has absorption in the blue region, where it has a high reflectance in the red region. The ratio 6/7 was used in this study for its ability to map kaolinite, montmorillonite and clay minerals. All these features have a high reflectance on band 6 and low reflectance in band 7 o ***http://www.sc.chula.ac.th/courseware/2309507/Lecture/remote18.htm*** f Landsat 8 image. The ratio 6/5 was used for mapping ferrous minerals due to the high reflectance of these minerals in this ratio (***R. Gupta., 2003***).

Two combinations of RGB images have been used for lithological mapping and hydrothermal alteration zones which they called Sabin's ratio (4/2, 6/7 and band 10 as RGB and 4/2, 6/5 and 6/7 as RGB) (***F. Sabins,1999***)

Identification of iron oxides is implemented using bands 2 and 4 of Landsat-8. Mapping clay and carbonate minerals is carried out using bands 6 and 7 of Landsat-8. Band ratios derived from image spectra (4/2, 6/7, 5/4 in RGB) is used for the identification of rock units, alteration. The alteration minerals are detected in the scenes as yellow color. Other interesting data on this issue follows.

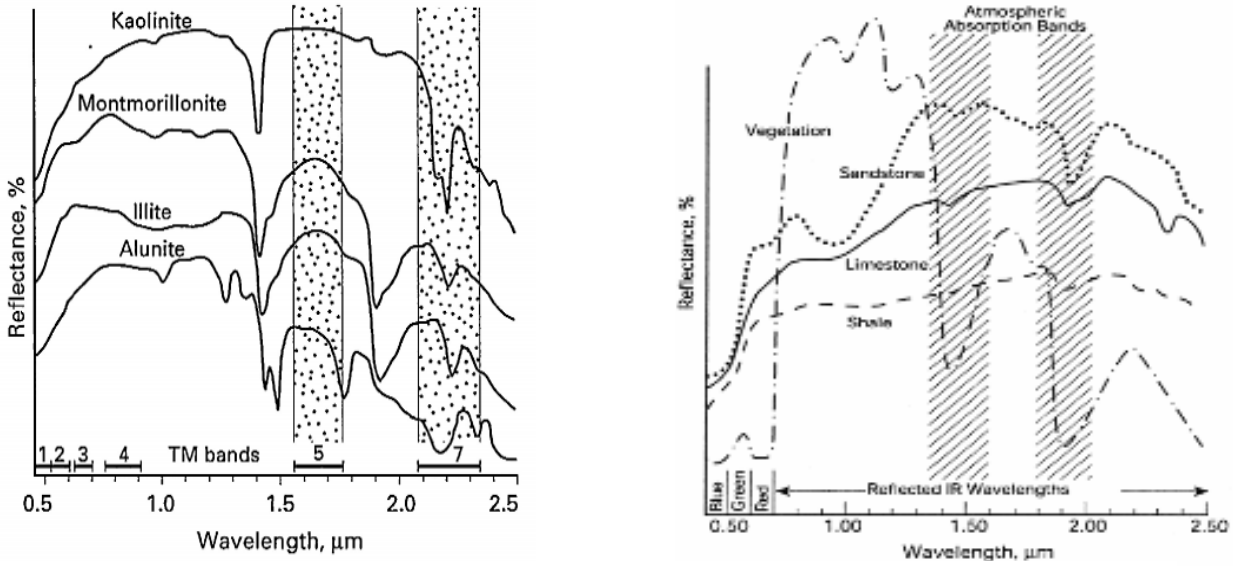


*Figure 12. Spectral signatures (F. Sabins, 1999)*

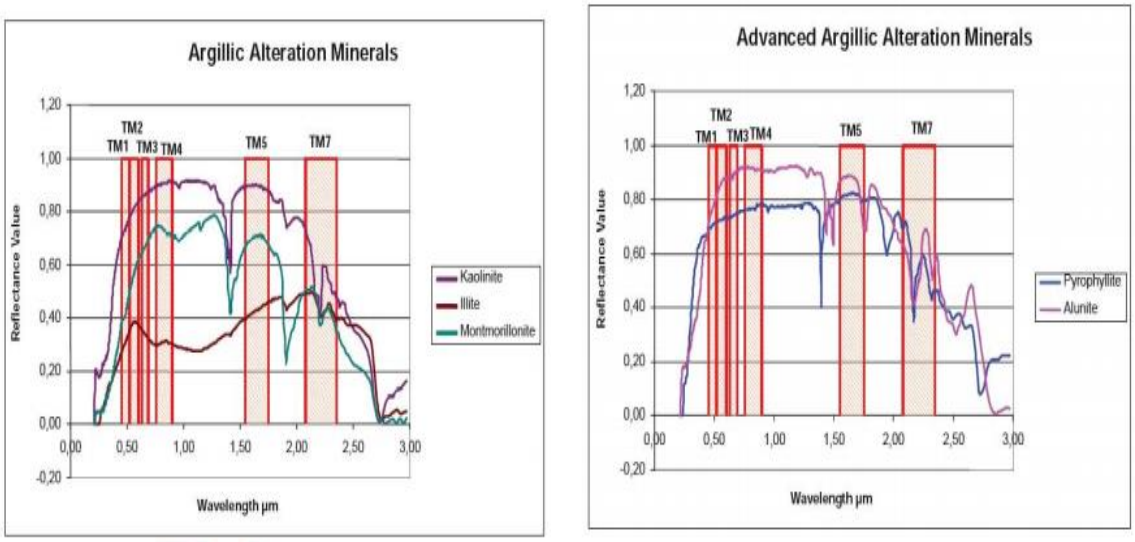


*Figure 13 Landsat 8 spectral signatures*

*(M. Yadzi, 2013)*

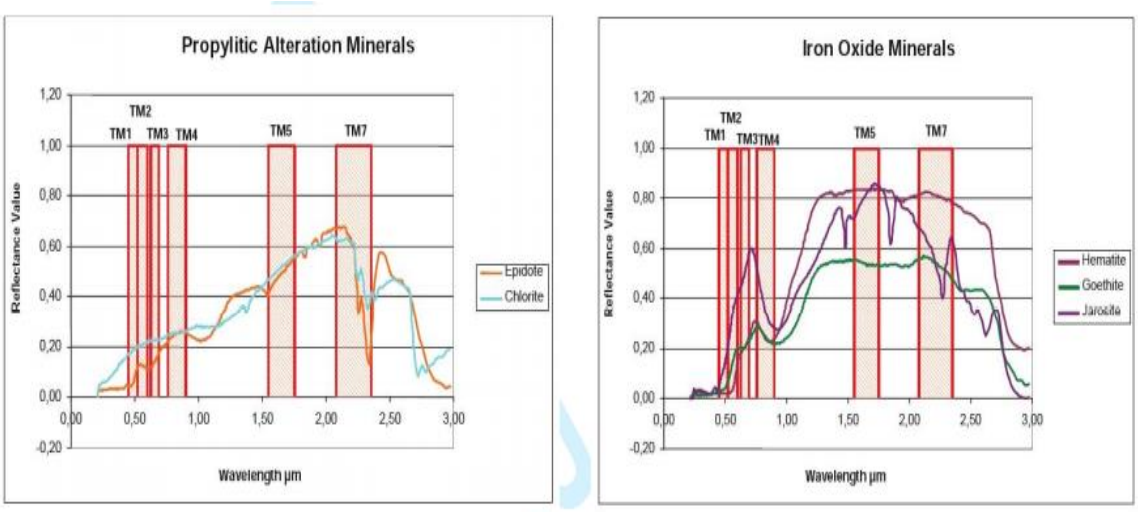


*Figure 14 Landsat 8 spectral signatures for alteration minerals*

*(M. Yadzi, 2013)*

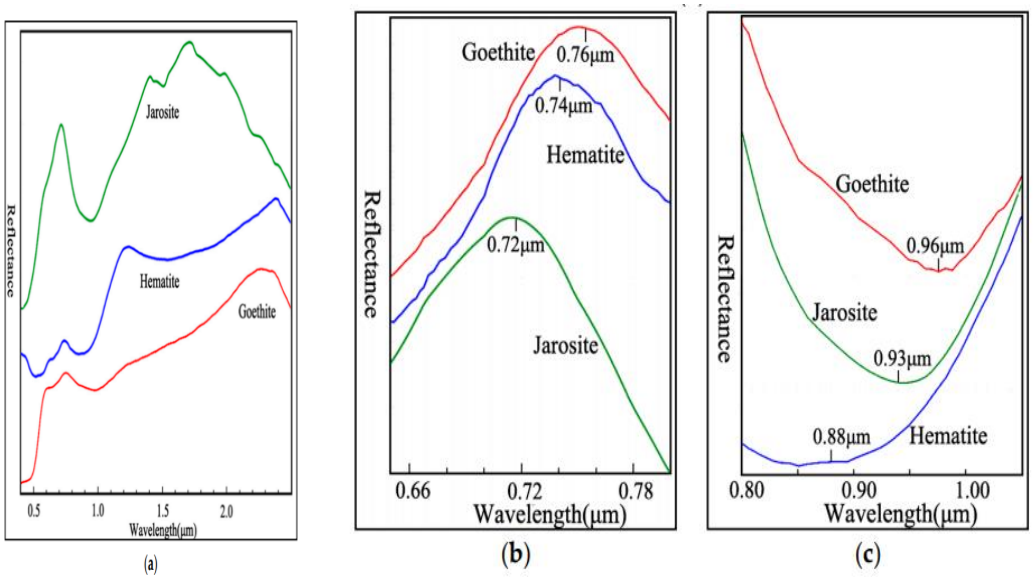


*Figure 15 Sentinel-2 spectral signatures (G. Wenyan, 2020)*

If individual bands provide useful information for specific types de mineral species, the triad RGB should provide much more information, Figure 11 (***G. Wenyan et al, 2020***).

Hydrothermal alteration is a very complex process involving mineralogical, chemical and textural changes, resulting from the interaction of hot aqueous fluids with the rocks through which they circulate, under evolving physicochemical conditions. Hydrothermal fluids chemically attack the mineral constituents of the wall rocks, which tend to re- equilibrate by forming new mineral assemblages that are in equilibrium with the new conditions. As a result of one of these processes, Escondida became a multi-stage composited mine district subjected to a hydrothermal alteration whose structural features are typically associated with mineralizations where propyllitic (epidote, chlorite, calcite), argillic (kaolinite, quartz, montmorillonite), phyllic (quartz, sericite, pyrite), potassic (biotite, sericite, felspar, quartz) components and others are typical mineral specimens associated with porphyry copper deposits**.** (***Porter GEO, 2021***)